7706 J. Med. Chem. 2009, 52, 7706–7723
DOI: 10.1021/jm900713y

Journal of Medicinal Chemistry Article

Increasing Selectivity of CC Chemokine Receptor 8 Antagonists by Engineering Nondesolvation Related Interactions with the Intended and Off-Target Binding Sites

Igor Shamovsky,*[,†] Chris de Graaf,[#,○] Lisa Alderin,[†] Malena Bengtsson,[†] Håkan Bladh,[†] Lena Börjesson,[†] Stephen Connolly,[§] Hazel J. Dyke,[⊥] Marco van den Heuvel,[⊥] Henrik Johansson,[†] Bo-Göran Josefsson,[†] Anna Kristoffersson,[†] Tero Linnanen,[†,◆] Annea Lisius,[†] Roope Männikkö,[∥,¶] Bo Nordén,[†] Steve Price,[⊥] Lena Ripa,[†] Didier Rognan,[#] Alexander Rosendahl,[‡] Marco Skrinjar,[†] and Klaus Urbahns[▽]

[†]*Department of Medicinal Chemistry and* [‡]*Department of Biological Sciences, AstraZeneca R&D Lund, S-22187 Lund, Sweden,* [§]*Department of Medicinal Chemistry, AstraZeneca R&D Charnwood, Loughborough, Leicestershire LE11 5RH, U.K.,* [∥]*Department of Safety Pharmacology, Safety Assessment U.K., AstraZeneca R&D Alderley Park, Macclesfield SK10 4TG, U.K.,* [⊥]*Argenta Discovery Ltd, 8/9 Spire Green Centre, Flex Meadow, Harlow, Essex CM19 5TR, U.K.,* [#]*Structural Chemogenomics Group, Laboratory of Therapeutic Innovation, UMR 7200 CNRS-UdS (Université de Strasbourg), 74 Route du Rhin, B.P. 24, F-67400 Illkirch, France, and* [▽]*Global Respiratory and Inflammation Research, AstraZeneca R&D Charnwood, Loughborough, Leicestershire LE11 5RH, U.K.* [○]*Current address: Division of Medicinal Chemistry, Faculty of Sciences, Leiden/Amsterdam Center for Drug Research, VU University Amsterdam, De Boelelaan 1083, 1081 HV Amsterdam, The Netherlands.* [◆]*Current address: FeF Chemicals A/S, Københavnsvej 216, 4600 Køge, Denmark.* [¶]*Current address: Department of Physiology, Anatomy and Genetics, Sherrington Building, University of Oxford, Parks Road, Oxford OX1 3PT, UK.*

Received May 26, 2009

The metabolic stability and selectivity of a series of CCR8 antagonists against binding to the hERG ion channel and cytochrome Cyp2D6 are studied by principal component analysis. It is demonstrated that an efficient way of increasing metabolic stability and selectivity of this series is to decrease compound lipophilicity by engineering nondesolvation related attractive interactions with CCR8, as rationalized by three-dimensional receptor models. Although such polar interactions led to increased compound selectivity, such a strategy could also jeopardize the DMPK profile of compounds. However, once increased potency is found, the lipophilicity can be readjusted by engineering hydrophobic substituents that fit to CCR8 but do not fit to hERG. Several such lipophilic fragments are identified by two-dimensional fragment-based QSAR analysis. Electrophysiological measurements and site-directed mutagenesis studies indicated that the repulsive interactions of these fragments with hERG are caused by steric hindrances with residue F656.

Introduction

Chemokines constitute a family of small secreted peptides, which control the trafficking cascades of leukocytes to inflammatory sites. They act through binding to specific high-affinity receptors, the chemokine receptors, which belong to a superfamily of G-protein-coupled receptors (GPCRs[a]). The chemokine receptor family is the largest subfamily of known peptide-binding GPCRs.[1] They belong to the class A GPCRs, which also include rhodopsin, β_1-adrenergic, β_2-adrenergic, and A_{2A} adenosine receptors, four GPCRs for which high-resolution X-ray crystal structures have been solved.[2−5] The chemokine system regulates the development, activation, and recruitment of leukocytes and plays important roles outside the immune system.[1]

A wealth of structure−activity relationships and mutagenesis studies on the class A GPCR antagonists suggests that there is a generic binding pocket for small molecules inside the heptahelical bundle common to this subfamily. With the release of crystal structures of the bovine rhodopsin,[2] it is apparent that this generic transmembrane (TM) binding pocket for small molecules is reminiscent of the retinal-binding pocket in rhodopsin.[6,7] The predicted high value of homology modeling of GPCRs in the identification of the class A GPCR ligands[6,7] has been verified in several classes of therapeutics,[8] although intrinsic conformational plasticity inherent in GPCR structure and ligand binding sites has to be taken into consideration.[9]

The pro-inflammatory chemokine receptor 8 (CCR8) is selectively expressed on a subset of T-helper-2 (Th2) cells, eosinophils, and on monocyte derived dendritic cells, and is upregulated upon activation.[10,11] These effector cells migrate to the site of inflammation by sensing a gradient of the chemokine CCL1 by the cell surface expressed CCR8 receptor. Once inside the inflamed tissue, the CCR8 positive cells arrest and perform their effector function. Among other functions, the activated Th2 cells produce the key cytokines IL-4, IL-5, and IL-13, which are the predominant mediators in inflammation and hyperresponsiveness in bronchial asthma and atopic dermatitis. Clinical studies have demonstrated significantly elevated numbers of CCR8 positive cells in asthmatics and atopic dermatitis patients.[12−14] The pivotal role of CCR8 in driving allergic diseases like asthma was

*To whom correspondence should be addressed. Phone: +4646-338347. Fax: +4646-338399. E-mail: igor.shamovsky@astrazeneca.com.

[a]Abbreviations: CCR8, CC chemokine receptor 8; DMPK, drug metabolism and pharmacokinetics; hERG, human ether-à-go-go-related gene; GPCR, G-protein-coupled receptor; LLE, ligand lipophilicity efficiency; PCA, principal component analysis; H-bond, hydrogen-bond; TM, transmembrane; TM7, transmembrane α-helix number 7; Cyp2D6, the 2D6 isoform of cytochrome P450; DSM, discrete structural modifications; LMP2, local Møller−Plesset second-order perturbation theory calculation; cc-pVTZ(-f), the Dunning correlation consistent polarized valence triple-ζ basis set without *f*-functions; IFP, interaction fingerprint bit-string; PLS-DA, partial least-squares discriminant analysis.

 Published on Web 07/17/2009

Figure 1. Core structure of CCR8 antagonists. R1 is normally a lipophilic group; R2 is normally a polar group.

demonstrated in CCR8 deficient mice, in which it was shown that CCR8 knock-down significantly ameliorated lung inflammation and airway function in several allergic airway models.[15,16] These clinical and experimental results strongly suggest that CCR8 antagonists could be of therapeutic value in allergic pulmonary diseases.[17,18]

The vast majority of nonpeptide chemokine receptor antagonists share a common pharmacophore, which includes lipophilic groups and a centrally located protonated amine[18,19] that forms an ionic bond with the conserved glutamate $E^{7.39}$ of chemokine receptors.[20,21] Different classes of known small-molecule CCR8 antagonists also reveal this general pharmacophore.[17,18,21−24] This particular pharmacophore is also inherent in hERG ion channel blocking agents[25−27] and in inhibitors of the 2D6 isoform of cytochrome P450 (Cyp2D6),[28] one of the most important enzymes involved in drug metabolism. Indeed, much of the preclinical attrition of chemokine receptor antagonists has been due to the challenges of increasing selectivity against hERG and Cyp2D6, and metabolic liability.[29−34]

In this communication, we consider a series of 464 CCR8 antagonists, which are based on the 3,9-diazaspiro-[5.5]undecane scaffold (Figure 1).[22] Apart from general binding of these compounds to the hERG ion channel, several compounds of this series also exhibit binding to Cyp2D6 and have poor metabolic stability. The overall promiscuity of bioactive compounds is thought to be related to their lipophilicity, typically quantified by Log *P* or Log *D*.[35] A main focus of this study is to investigate the connection of the intended and off-target binding of the CCR8 antagonists with their lipophilicity. We demonstrate that engineering attractive polar interactions in this series of CCR8 antagonists with the primary binding site results in an increase in potency and a simultaneous decrease in lipophilicity, which in turn diminishes lipophilicity-linked promiscuous interactions and also increases metabolic stability. Both location and conformational flexibility of key polar residues lining the consensus TM binding pocket[36] within the CCR8 homology model are shown to be critical to explain the structure−activity relationships and to guide the intended decrease of compound lipophilicity. However, although the reduction of the desolvation related component of potency[37−41] is a reliable general approach to increase compound selectivity,[35,42,43] this strategy can have certain limitations caused by poor permeability and bioavailability of polar compounds. In addition, contrary to the general strategy of reducing lipophilicity, it has also been demonstrated that in specially identified locations polar functionality may form detrimental intrinsic attractive interactions within the hERG ion channel cavity[26,42−44] and therefore decrease selectivity against hERG. In a previous communication,[44] we demonstrated that molecular fragments, which are responsible for both beneficial and detrimental nondesolvation related interactions[40] with an antitarget, can be identified by two-dimensional fragment-based QSAR analysis. We identified structural features of chemokine receptor antagonists that caused intrinsic attractive interactions with hERG leading to the loss of hERG selectivity, whereas here we explore possibilities for anti-hERG propensity of spirocyclic CCR8 antagonists. The structures of these CCR8 antagonists **1**−**30** are detailed in Table 1 and Table S1 of Supporting Information. The molecular basis of repulsive interactions with the hERG ion channel is revealed by electrophysiological experiments conducted with a focused set of 25 of these compounds and eight hERG mutants. It is shown that some lipophilic fragments built in to these CCR8 antagonists, which are responsible for high intrinsic anti-hERG propensities, do not fit to the narrow part of the channel between residues F656.

Methods

Synthesis. The compounds were prepared according to Route A (Scheme 1) by reductive amination of *tert*-butyl 3,9-diazaspiro[5.5]undecane-3-carboxylate hydrochloride **31** followed by amide coupling with a suitable acid after deprotection. Alternatively, compounds were prepared according to route B (Scheme 2) by amide coupling of compound **31**, followed by deprotection and subsequent reductive amination to afford the desired compound. Compound **30** was prepared by alkylation of **31** with 5-bromo-7-(bromomethyl)-3,3-difluoro-2,2-dimethyl-2,3-dihydro-1-benzofuran **38** according to Scheme 3. The intermediate **38** was synthesized via alkylation of *ortho*-cresol **32**, followed by intramolecular Friedel−Crafts acylation to afford the benzofuranone **35**. The ketone was transformed to the corresponding 1,3-dithiolane and the fluorine atoms were introduced through geminal difluorination. Under these reaction conditions, a bromine atom was also introduced in the aryl ring to form **37**. Following a radical bromination of the benzylic position and coupling with compound **31** to afford **39**, the bromine atom was removed by hydrogenation to give compound **40**. Deprotection and coupling with 5-aminopyridine-2-carboxylic acid gave the desired compound **30**. Synthetic details and characterization of the compounds can be found in ref 22 and in the Supporting Information.

Selectivity of CCR8 Antagonists through hERG Baseline Lipophilicity Relationships. Baseline lipophilicity relationships describe the link between compound lipophilicity (log *D*) and potency of binding (pIC_{50}) (eq 1).[37−40,45,46] Upon binding to the target or an off-target binding site, e.g., hERG, a hydrophobic drug molecule and the hydrophobic binding sites go through energetically favorable desolvation processes. Accordingly, the lipophilicity-driven term similarly adds to the overall binding potencies, both desired and undesired, as is expressed in eqs 1 and 2. Because binding sites in proteins normally represent hydrophobic clefts with few polar residues,[47,48] the hydrophobicity factors of binding sites rarely significantly deviate from 1,[45] although such deviations have been noted.[37] Correspondingly, the selectivity is virtually insensitive to compound lipophilicity per se but is determined by an interplay of nondesolvation related specific interactions with target and antitarget, such as H-bonding, $\pi-\pi$ interactions and geometric fit.[41,49] This point is clearly seen in a difference of the eqs 1 and 2.

$$pIC_{50}{}^{CCR8} = a^{CCR8} \log D - k\Delta G_{intr}{}^{CCR8} + \text{const} \quad (1)$$

$$pIC_{50}{}^{hERG} = a^{hERG} \log D - k\Delta G_{intr}{}^{hERG} + \text{const} \quad (2)$$

$$pIC_{50}{}^{CCR8} - pIC_{50}{}^{hERG} = \left(pIC_{50}{}^{CCR8} - a^{hERG} \log D\right) + k\Delta G_{intr}{}^{hERG} + \text{const} \quad (3)$$

$$k\Delta G_{intr}{}^{hERG} = -\left(pIC_{50}{}^{hERG} - a^{hERG} \log D\right) + \text{const} \quad (4)$$

Table 1. Structures of the Focused Set of Compounds[a]

No.	R1	R2	LogD	CCR8
1	3-phenoxyphenyl	4-chlorophenyl	3.50	7.72
2	2-phenoxyphenyl	4-chlorophenyl	3.50	7.09
3	2-(2-methoxyphenoxy)phenyl	4-chlorophenyl	3.40	7.46
4	2-isobutoxyphenyl	pyrimidin-4-yl	-0.11	6.85
5	2-isobutoxyphenyl	4-pyridyl	1.80	6.97
6	2-(2-methylprop-2-enoxy)phenyl	4-pyridyl	1.60	7.15
7	2-(1,1,2,2-tetrafluoroethoxy)phenyl	4-pyridyl	2.80	6.28
8	2-(2-methoxyphenoxy)phenyl	4-pyridyl	1.80	7.94
9	2-(2-methoxyphenoxy)phenyl	pyridin-4-yl-1-oxide	0.50	6.94
10	2-(2-methoxyphenoxy)phenyl	pyrimidin-4-yl	1.20	7.83
11	3-phenoxyphenyl	4-pyridyl	2.70	7.76
12	3-phenoxyphenyl	pyrimidin-4-yl	2.40	7.56
13	3-(2-methoxyphenoxy)phenyl	pyrimidin-4-yl	1.70	8.31
14	3-(2-methoxyphenoxy)phenyl	pyridin-4-yl-1-oxide	0.90	7.49
15	2-phenoxyphenyl	pyrimidin-4-yl	2.00	6.85
16	2-(2-methoxyphenoxy)phenyl	2-oxo-1H-pyridin-3-yl	0.90	7.26
17	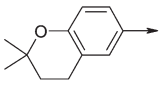	pyrimidin-4-yl	0.90	5.74
18	"	5-amino-2-pyridyl	1.10	7.02
19	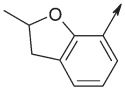	4-pyridyl	0.50	6.89
20	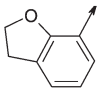	4-pyridyl	0.30	5.83
21	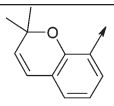	2-amino-4-pyridyl	1.50	8.25
22	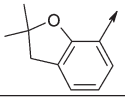	5-amino-2-pyridyl	1.00	8.58
23	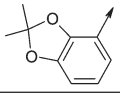	2-amino-4-pyridyl	1.20	8.18
24	"	3-amino-2-pyridyl	1.40	7.65
25	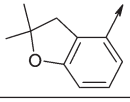	2-amino-4-pyridyl	1.40	7.65
26	"	5-amino-2-pyridyl	1.30	8.09
27	"	4-pyridyl	1.60	7.51
28	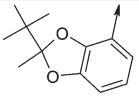	5-amino-2-pyridyl	2.60	8.55
29	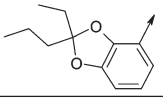	5-amino-2-pyridyl	2.50	8.62
30	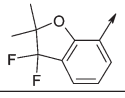	5-amino-2-pyridyl	2.30	8.58

[a] The common scaffold of the compounds is given in Figure 1. LogD denotes measured compound lipophilicity, where *D* is the apparent *n*-octanol/water partition coefficient, CCR8 is potency at CCR8 (pIC_{50}^{CCR8}).

Scheme 1. Route A[a]

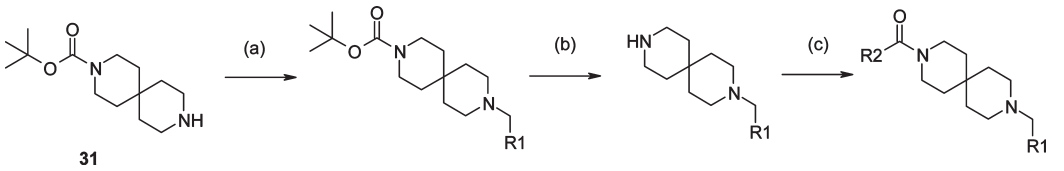

[a] Reagents and conditions: (a) R1-CHO, $NaBH(OAc)_3$, AcOH, DCM; (b) HCl, MeOH; (c) R2-COOH, HATU, NEt_3, DCM.

Scheme 2. Route B[a]

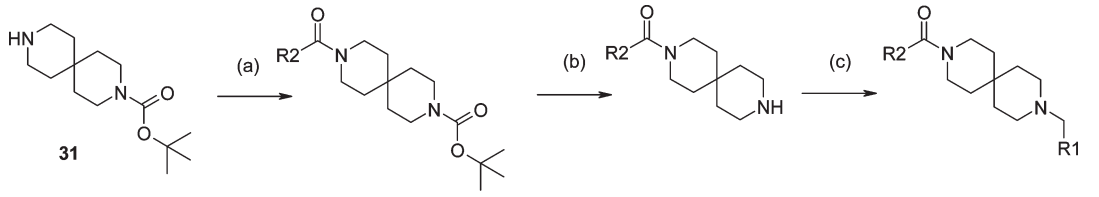

[a] Reagents and conditions: (a) R2-COOH, HATU, NEt_3, DCM; (b) HCl, MeOH; (c) R1-CHO, $NaBH(OAc)_3$, AcOH, DCM.

Scheme 3[a]

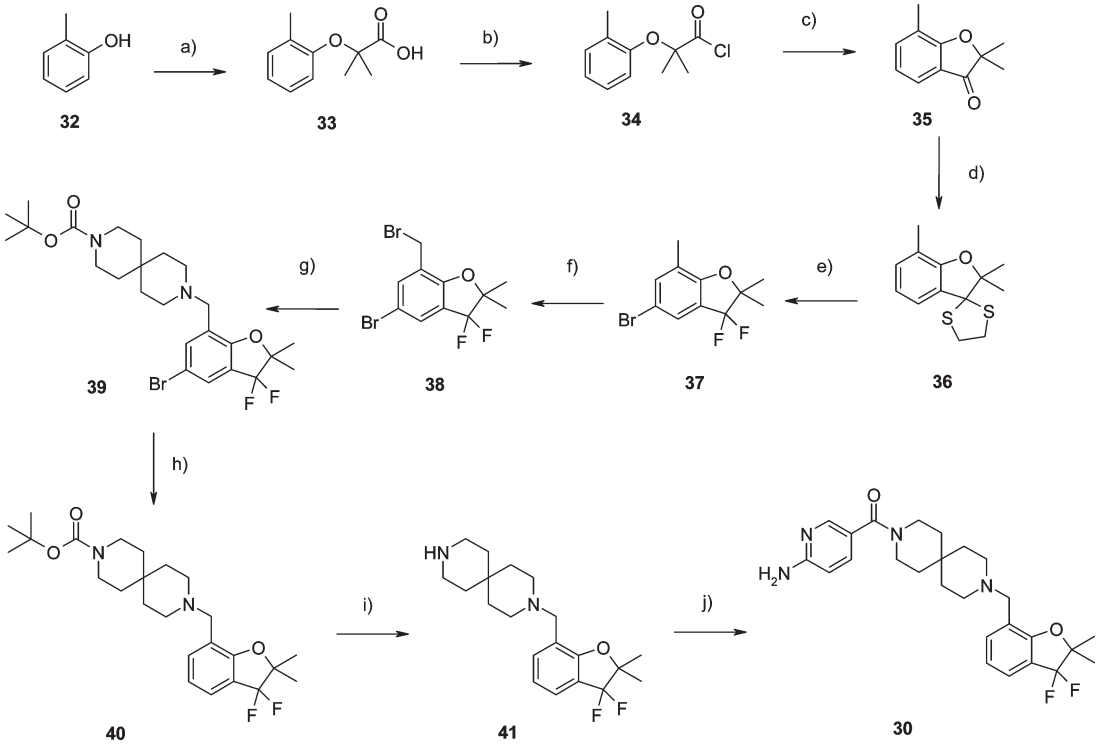

[a] Reagents and conditions: (a) (i) ethyl-2-bromoisobutyrate, potassium carbonate, DMF, (ii) NaOH, H_2O; (b) $SOCl_2$; (c) $AlCl_3$, toluene; (d) ethanedithiol, $BF_3 \cdot OEt_2$, $CHCl_3$; (e) 1,3-dibromo-5,5-dimethylhydantoin, 70% HF/pyridine complex, DCM; (f) *N*-bromosuccinimide, benzoylperoxide, CCl_4; (g) **31**, DIPEA, THF; (h) 10% Pd/C, H_2, MeOH; (i) TFA, DCM, H_2O; (j) 5-aminopyridine-2-carboxylic acid, PS-carbodiimide, HOBt, DCM.

where pIC_{50} is potency of a compound, D is the apparent *n*-octanol/water partition coefficient, a^{CCR8} and a^{hERG} are hydrophobicity factors of the corresponding binding sites, k is coefficient, equal to $(2.303RT)^{-1}$, and ΔG_{intr} is the intrinsic binding energy, which is not related to desolvation and describes direct interactions of the ligand with the binding site, including polar interactions and geometric fit.[40]

Expression 3 gives the compound selectivity against hERG. The two terms in the right side of eq 3 signify two approaches to increasing compound selectivity in a structural class. The first term increases when chemical alterations result in forming new direct attractive interactions with CCR8,[41,49] whereas the increase of the second term is an indication that new molecular fragments do not fit to hERG. Analysis of eq 3 is useful in lead identification and lead optimization projects only when the target and off-target proteins are not related, in which case it is possible to separate changes in the two terms. When the hydrophobicity factor of the binding site of an antitarget is close to 1, the first term of eq 3 is roughly equal to a previously described value of ligand lipophilicity efficiency, LLE.[35] The first term is not associated with any particular antitarget, correspondingly

the approach of increasing this term deals with general potential of compounds for multiple promiscuous interactions, in agreement with previous observations.[35]

It has been shown that the hydrophobicity factor of the hERG ion channel cavity, a^{hERG}, is indeed close to 1.[44] Correspondingly, according to eq 3, a normally expected average gain in hERG selectivity of compounds in chemical series is expected to be equal to the increase in the value of LLE. When the hydrophobicity factors of both target and antitarget binding sites are roughly equal, as in the present study, eq 3 is virtually free of desolvation effects and gives an opportunity to analyze the selectivity as an interplay of intrinsic interactions with the alternative binding sites. As opposed to the general character of the first term of eq 3, the second term, which is detailed in eq 4, is linked to a particular antitarget and represents an additional opportunity to improve selectivity in a chemical series by increasing the specific anti-antitarget propensity of compounds by engineering direct repulsive interactions with the binding site of this antitarget. Both terms of eq 3 are analyzed in the present study.

Molecular Modeling of CCR8 Receptor−Ligand Interactions. Construction of Three-Dimensional CCR8 Receptor Models. A ground-state homology model of the CCR8 receptor was constructed following a previously defined protocol.[50] A preliminary high-throughput receptor model, including only the seven TM helices, was derived from a validated CCR5 model[51] using the GPCRgen program.[52] The amino acid sequence alignments used for constructing the receptor models are shown in Figure S1 of Supporting Information. Notice that the Ballesteros−Weinstein residue numbering scheme[53] and a recently proposed numbering scheme of the extracellular loop 2[50] are used throughout the manuscript. Compound **13** (see Table 1) was docked into the receptor model using the "3 times speed-up" settings of the Gold v3.3 program, guided by experimentally driven H-bond constraints between the protonable tertiary amine of the diaza-spiro scaffold (Figure 1) and both $E^{7.39}$ carboxylate oxygen atoms. The active site center determined by the PASS program[54] was taken as the starting position of the GOLD flood fill algorithm. This preliminary model of CCR8 with bound **13** was used to construct the extracellular and intracellular loops and for further refinement of the receptor model by in vacuo energy minimization and molecular dynamics simulation in a solvated membrane layer as recently described.[55] The χ_2 torsion angles of $N^{5.39}$ and $N^{5.43}$ and χ_3 torsion angles of $Q^{2.60}$ and $Q^{45.49}$ of the final optimized CCR8 model were independently rotated by 180°, yielding 16 ($= 2^4$) unique receptor models.

Automated Docking of Diaza-spiro-alkane Antagonists. The 3,9-diazaspiro[5.5]undecane antagonists presented in Table 1 were automatically docked in the 16 CCR8 homology models as described in the preceding section. The binding pose of compound **13** was used to generate an interaction fingerprint (IFP) bit-string as previously described.[56] Seven different interaction fingerprints, namely (1) hydrophobic contact, (2) aromatic face-to-face, (3) aromatic edge-to-face, (4) donor−acceptor and (5) acceptor−donor H-bond interactions, (6) positive−negative, and (7) negative−positive ionic interactions, were used to define the IFP bit-string. The cavity used for the IFP analysis consisted of the following 13 residues: $Y^{1.39}$, $Q^{2.60}$, $S^{3.29}$, $Y^{3.32}$, $Y^{3.33}$, $Q^{45.49}$, $Y^{45.51}$, $N^{5.39}$, $M^{5.42}$, $N^{5.43}$, $F^{6.51}$, $L^{6.55}$, and $E^{7.39}$. Eight residues of this set have been shown to be involved in ligand binding to CCR8.[21] The H-bond acceptor and donor interaction fingerprint bits of $Q^{2.60}$, $Q^{45.49}$, $N^{5.39}$, and $N^{5.43}$ were adapted to the side-chain amide rotamer of the receptor model, depending on whether the amide oxygen (H-bond acceptor) or nitrogen (H-bond donor) atom was facing the binding pocket, yielding 16 different IFPs corresponding to the 16 different receptor models. The reason for this was to account for protein flexibility and the existence of both H-bond acceptor and H-bond donor functional groups in the ligand (Table 1 and Table S1 of Supporting Information). For each of the diaza-spiro-alkanes, docking poses with the highest IFP similarity score and forming an H-bond-assisted salt bridge with $E^{7.39}$ were selected as representative binding modes.

Site Directed Mutagenesis Experiments of the hERG Ion Channel. Generation of hERG Mutant/Wild-Type hERG Expressing Cell Lines. The hERG gene was cloned into the pTight expression vector (Clonetech Laboratories, Inc., Mountain View, CA) to keep expression of the channel under tetracycline control. The mutations T623S, S624A, S624T, Y652A, Y652F, F656M, F656T, and F656W were introduced into the gene by standard polymerase chain reaction (PCR)-based site-directed mutagenesis techniques (QuickChange, Stratagene, La Jolla CA) and confirmed by sequencing both strands of the entire gene. Linearized hERG DNA was transfected into Tet-On CHO K1 cells together with a linear hygromycin selection marker using the lipofectamine method (Invitrogen). Cells were then incubated in presence of 0.6 mg/mL hygromycin until cells in untransfected control flask had died (2−3 weeks). Cells were then incubated in the presence of 0.8 μg/mL doxycyclin for 24−48 h to induce channel expression, which was confirmed using the IonWorks HT high-throughput electrophysiology measurement platform (Molecular Devices, Sunnyvale CA).[57] Clonal cell lines were then created by dilution cloning and selected by measuring functional expression, using IonWorks HT.

Pharmacological Comparison. An automated, plate-based electrophysiology device (IonWorks HT)[57] was used to study the pharmacological profile of wild-type hERG (wt-hERG) channel and each hERG mutant by directly assessing the channel function.[58] For each experimental run of IonWorks HT, the device made perforated whole-cell recordings at 21 °C, usually from more than 200 of the 384 wells in a 384-well substrate (Molecular Devices). The extracellular solution was Dulbecco's phosphate-buffered saline containing calcium (0.9 mM) and magnesium (0.5 mM) (PBS; Invitrogen) and the "pipette" solution was (in mM): KCl 140, EGTA 1, $MgCl_2$ 1 and HEPES 20 (pH 7.25−7.30 using 10 M KOH) plus 100 μg/mL amphotericin B (Sigma-Aldrich). After attainment of the whole-cell configuration, a precompound hERG current was evoked in each cell in the presence of PBS by the following voltage protocol: a 20 s period holding at −70 mV, a 160 ms step to −60 mV (to obtain an estimate of leak), a 100 ms step back to −70 mV, a 1 s step to +40 mV, a 2 s step to −30 mV, and finally a 500 ms step to −70 mV. The amplitude of the hERG current was measured by subtracting the baseline current at −70 mV from peak current measured during the step to −30 mV. Test compounds, vehicle, or 31.6 μM terfenadine controls were then added to each well, and after 3 min, the voltage pulse was reapplied to generate a postcompound hERG current. Terfenadine at 31.6 μM fully blocked currents in wt-hERG and all hERG mutants in our setup. In between the pre- and

postcompound voltage pulses, there was no clamping of the membrane potential.

Compounds to be tested were first dissolved in DMSO at a concentration 300-fold the top test concentration and then diluted to the final test concentrations. IonWorks HT is set up such that each well of a 96-well plate containing the test compounds maps to four wells of the 384-well substrate in which recordings are made. The 96-well compound plate was made up of two identical halves. Each half was made up of PBS containing eight half log-spaced concentrations of a single test compound at 3-fold its final concentration, and this was repeated five times. For the remaining eight wells of the half plate, four contained 1% DMSO and four contained 95 μM terfenadine. Each well of a 384-well substrate initially contained 3 μL of PBS and 3 μL of PBS containing a cell suspension of a single cell line at a concentration of 250000 cells/mL. When 3 μL of test compound from the compound plate was added to each well of a 384-well substrate, this meant that the cells were exposed to the final compound test concentration, 0.33% DMSO or 31.6 μM terfenadine.

For each IonWorks HT run, the hERG tail current amplitude in each cell in the presence of PBS was compared with that in the presence of test compound for the same cell. All the data were then scaled by defining the effect of 0.33% DMSO as 0% inhibition and the effect of the supramaximal blocking concentration of terfenadine as 100% inhibition. Because the contents of each well of the test plate were added to four wells of the 384-well substrate, there could be percentage inhibition data from between 0 and 4 cells for each test concentration. Because only one compound was tested in a 384-well substrate containing wt-hERG and a hERG mutant cell line, each point of the noncumulative curve came from up to 20 cells. The pharmacological data were fitted using a four parameter nonlinear regression (curve top, curve slope, and IC_{50} value, with the curve bottom being normalized to 0) with in-house Origin package.

Results and Discussion

Multivariate Analysis of Properties of CCR8 Antagonists. An analysis of CCR8 antagonists of the general structure depicted in Figure 1 indicated that the following unwanted properties are inherent in many compounds of this class: inhibition of the hERG potassium ion channel, inhibition of Cyp2D6, and high microsomal and hepatic metabolic clearance. Therefore, the lead optimization strategy in this class was predominantly focused on increasing compound selectivity toward CCR8 and against these properties. Principal component analysis (PCA) of relevant properties of a series of 464 compounds of the structural class under study was performed by the program SIMCA-P+ (version 11; Umetrics, Kinnelon, NJ) to define the most efficient way to separate the intended potency from the unwanted properties. Figure 2 illustrates the plot of loadings of PCA, which represents the projections of the initial coordinate system of scaled compound properties into the plane of two first eigenvectors (PC-1 and PC-2) of the covariance matrix. The center of the coordinate system corresponds to the average values of properties. This plot illustrates major correlations that exist between properties in the data set. As is seen, the subset of descriptors of desired properties (shown in green) is grouped together and roughly occupies the third quadrant of the plot. This subset includes the primary potency at CCR8

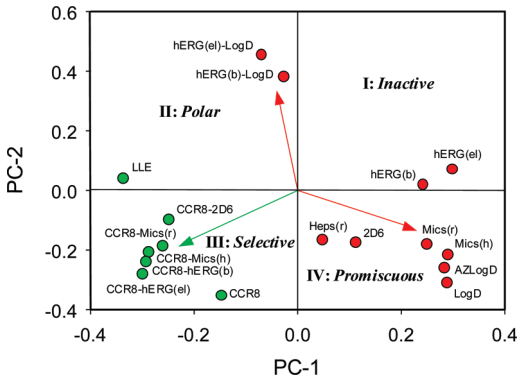

Figure 2. The main loadings plot of the PCA of properties of 464 in-house CCR8 antagonists of the common scaffold indicated in Figure 1. Each compound was described by 17 properties. PC-1 and PC-2 represent the first and the second principal components of the covariance matrix. Projections of coordinate axes of intended properties are shown in green, those of unwanted properties in red. Labels CCR8, hERG(b), hERG(el), and 2D6 designate potencies in logarithmic units at CCR8, at hERG in binding experiments, at hERG in electrophysiological experiments, and at Cyp2D6 in binding assay, respectively. Labels LogD and AZLogD are measured and predicted compound lipophilicities at pH = 7.4, respectively. Labels Mics(h), Mics(r), and Heps(r) are rates of metabolic clearance in logarithmic units in human miscosomes, rat microsomes and rat hepatocytes, respectively. Labels CCR8-hERG(b), CCR8-hERG(el), CCR8−2D6, CCR8-Mics(h), and CCR8-Mics(r) are the corresponding selectivities. Labels LLE, hERG(b)-LogD, and hERG(el)-LogD are nondesolvation related components of potencies at CCR8, hERG in binding experiments, and hERG in electrophysiological experiments, respectively. Locations of majority of promiscuous, inactive, polar, and selective compounds are indicated. The arrows designate structural alterations within the compound class that usually result in lipophilicity-linked promiscuous binding (quadrant IV), specific binding to the primary target (quadrant III), or specific binding to the hERG ion channel (quadrant II). The first two components in the PCA plot explain 70% of the variance.

(pIC_{50}^{CCR8}) and selectivities against undesirable binding, i.e., differences between the primary potency and unwanted properties such as off-target potencies or rates of metabolic clearance expressed in logarithmic units. Statistically, compounds that fall in this parameter space exhibit both high primary potency and high selectivities. The opposite parameter space, which is located in the first quadrant, refers to relatively inactive compounds.

The subset of descriptors of unwanted properties (shown in red) includes potency of hERG binding and potency of inhibition of hERG in the electrophysiological assay, potency of inhibition of Cyp2D6, and rates of microsomal and hepatic metabolic clearance. In addition, measured and calculated compound lipophilicity at pH = 7.4 (LogD and AZLogD, respectively), ligand lipophilicity efficiency (LLE), and intrinsic hERG-binding propensity (potency at hERG minus Log *D*)[44] have been added to the set of properties for PCA. As is seen in Figure 2, the majority of unwanted descriptors, including binding to and inhibition of the hERG ion channel, inhibition of Cyp2D6, and metabolic instability in microsomes and hepatocytes, are grouped together in the fourth quadrant, which indicates that this particular space represents the area of promiscuity. In addition to the unwanted properties, this area also includes descriptors of compound lipophilicity, LogD and AZLogD, which suggests that the fourth quadrant of the plot is the common place of the most lipophilic compounds in the set.

This implies that lipophilicity of the CCR8 antagonists correlates with their binding to multiple antitargets such as hERG and metabolic enzymes because of high contribution of nonspecific hydrophobic interactions to the off-target binding affinities, which is in line with previous observations.[35,37,59,60]

Descriptors of two unwanted properties, namely intrinsic potency for binding to and inhibition of the hERG channel, are located in the PCA plot far beyond the area of promiscuity, in the second quadrant, which is the common place for relatively polar compounds. The results suggest that an increase of polarity of compounds moves them away from the area of promiscuity toward the second quadrant in the plot. Although this allows one to get rid of desolvation-linked promiscuous off-target binding, it does not increase the required selectivities because the desolvation effects similarly decrease binding affinity at the primary target (see eqs 1 and 2). On the other hand, the intended selectivities are colocated in the PCA plot with LLE, which suggests that increasing polarity while maintaining the required level of the primary potency is the most efficient way of increasing selectivity against promiscuous interactions, which is in agreement with current opinion.[35,41,49] The key to this path is to find new direct attractive interactions with the primary target in the form of H-bonding, $\pi-\pi$ interactions, or improved geometric fit.[41,44,49] This path, shown in Figure 2 by the green arrow, results most of the time in reducing compound lipophilicity, which has clear limitations. It is well recognized that compound lipophilicity has to be within a certain interval to maintain the required DMPK profile of drug candidates, including bioavailability and permeability. In addition, an increase of the number of polar functions in compounds, designed to lead to more potency at the intended target, may also lead to polar interactions with binding sites of antitargets and thereby not result in increased selectivity.[26,39,42−44] Specifically, it has been noted that general pharmacophores of chemokine receptor antagonists are similar to that of the hERG ion channel blockers such that accumulation of solubilizing groups on one side of the molecule often leads to the loss of hERG selectivity because of polar interactions within the hERG channel vestibule cavity.[42,43] A distinctive sign of similarity of pharmacophores for direct attractive interactions in CCR8 and hERG within the considered compound class is the fact that the descriptors of such interactions (denoted as LLE and hERG-LogD, respectively) are colocated in the second quadrant of the PCA plot in Figure 2.

Furthermore, introduction of direct attractive interactions of polar functional groups of compounds to increase selectivity may also bring unexpected problems with intrinsic metabolic clearance or inhibition of metabolic pathways by interacting positively with the active sites of metabolic enzymes.[37−39,61−63] In this case, it is valuable to be able to increase compound selectivity against a specific antitarget without lowering lipophilicity. This can be done by disrupting existing polar interactions or by introducing steric incompatibility with the antitarget, which increases the anti-antitarget propensity (eq 4). This strategy, which addresses the issues linked to one particular antitarget, is widely used in lead optimization. The method of discrete structural modifications (DSM) of reducing hERG liability[43] and a common practice of removing metabolically vulnerable spots in compounds to increase metabolic stability[64] are just two examples of nondesolvation related increasing of intrinsic anti-antitarget propensities.

The major correlations between descriptors in the series of CCR8 antagonists revealed by the PCA work in a statistical sense, which leaves many outliers, both good and bad, out of the picture. At the same time, it is in the outliers, where potential value might be found. The next section deals with special structural features of CCR8 antagonists that make them particularly effective in increasing hERG selectivity.

Detection of Nondesolvation Related Interactions with the CCR8 and the hERG Binding Sites. A subset of 30 spirocyclic CCR8 antagonists with diverse R1 and R2 fragments were chosen to form a focused set for detailed investigation. All types of fragments that maintained the primary potency of compounds below 2 μM were included in the set. Molecular structures and experimental data obtained for this set are presented in Tables 1, 2, and Table S1 of the Supporting Information. The two-dimensional fragment-based QSAR analysis utilizing eq 3 was carried out to detect intrinsic interactions with CCR8 and hERG in this data set. As suggested in our previous communication,[44] average contributions of different molecular fragments R1 and R2 to the LLE and to the hERG selectivity were calculated by solving the Free−Wilson system of equations[65] using an in-house AstraZeneca plug-in of the program Spotfire DecisionSite (version 9.1; TIBCO Spotfire, Göteborg, Sweden). The central assumption of the Free−Wilson approach, independent contributions of R1 and R2 to compound properties, is unequivocally accepted in this study. The objective was to find direct attractive interactions with the target binding site and direct repulsive interactions with hERG as required by eq 3.

Figure 3 gives the results of the two-dimensional QSAR analysis. Relative contributions of each molecular fragment of the focused set to attractive nondesolvation related interactions of compounds with the binding sites of CCR8 and hERG are quantified by LLE and ($pIC_{50}^{hERG} - \log D$), respectively. Structures of the fragments R1 and R2 are presented in Figure 4. Consistent with eq 3 and 4, this plot visualizes an interplay of direct interactions with the binding sites of the target and the antitarget, with desolvation-driven components of the corresponding potencies being taken out of the picture. The diagonal line, called the average hERG lipophilicity baseline, signifies the average fit of fragments in the data set to the hERG channel cavity. Consistent with eq 3, the line illustrates how a fragment, either R1 or R2, with an average intrinsic hERG-binding propensity, contributes to the hERG selectivity of compounds depending on its intrinsic fit to the primary target. Fragments that exhibit unusually high hERG-binding propensities are located below the line, whereas those fragments that make unusual repulsive interactions with the hERG cavity are above the line. The vertical line is the average CCR8 lipophilicity baseline or the average LLE line, which splits all fragments into two groups such that the fragments located to the left and to the right from this line form less and more efficient direct interactions with the CCR8 binding site than an average fragment, respectively. The resulting nonorthogonal coordinate system divides the plot into four quadrants, with the fragments located in the first two quadrants being the main focus of the present investigation.

The fragments are classified in Figure 4. Those that appear in the first quadrant have the highest potential for selective interactions with the primary target not only because they fit to the primary target and do not fit to the hERG channel but also because they are less prone to desolvation-linked

Table 2. Potencies at hERG and hERG Mutants of the Focused Set of Compounds[a]

No.	hERG el-phys	hERG binding	T623S	S624A	S624T	Y652A	Y652F	F656M	F656T	F656W
1	6.22	7.09	0.60	0.77	0.10	0.42	−0.73	0.42	0.46	0.39
2	7.08	8.19	0.91	0.93	0.48	0.53	−0.14	0.78	1.32	−0.08
3	7.06	8.6	0.81	0.42	0.08	0.71	−0.20	0.11	0.81	−0.30
4	5.31	4.72	0.22	0.51	0.12	0.70	−0.42	0.21	1.65	−0.42
5	5.72	4.82	0.22	0.47	−0.10	1.04	−0.64	0.39	1.82	−0.87
6	5.63	5.96	0.08	0.27	0.20	0.74	−1.07	0.23	2.26	−0.60
7	5.29	4.77	0.06	0.11	−0.08	1.00	−0.32	0.48	1.42	−0.54
8	7.34	7.52								
9	6.66	6.68								
10	7.15	6.92	0.94	0.58	1.20	1.79	−0.16	0.18	1.49	−0.03
11	6.35	6.44								
12	5.71	5.85	−0.03	0.56	−0.25	0.67	−0.01	−0.21	0.22	−0.57
13	5.72		0.44	0.67	−0.30	0.98	−0.29	−0.20	0.58	−0.15
14	4.59	5.07	0.39	0.29	−0.28	1.61	−0.35	−0.20	0.87	−0.39
15	6.64		1.16	0.72	0.53	0.79	−0.48	0.21	1.23	−0.16
16	4.85	5.7	0.51	0.54	0.24	1.19	0.35	0.22	1.92	−0.18
17	4.95		0.39	0.74	−0.39	0.82	0.11	−0.30	0.46	−0.14
18	4.71	4.49	0.24	1.09	−0.28	0.83	0.47	−0.66	−0.09	−0.35
19	4.68	5.09	0.24	0.61	−0.12	1.63	−0.21	1.04	1.41	−0.58
20		5.11								
21	4.42		0.20	0.48	−0.62	0.93	0.04	0.37	1.32	−0.75
22	4.36	4.43	0.22	0.82	−0.05	0.83	0.35	−0.31	0.51	−0.99
23	4.78	6.12	−0.06	0.59	−0.33	1.22	−0.19	0.62	1.37	−0.39
24	5.38	4.49	0.41	1.32	0.43	1.81	0.64	−0.26	0.77	−0.32
25	4.54	4.77	0.01	0.55	−0.58	0.89	−0.37	0.14	1.32	−0.61
26	4.78	4.89	0.49	0.79	0.31	1.23	0.68	−0.22	0.20	−0.66
27	5.15	4.52								
28	4.95	4.51	0.11	0.70	0.00	0.39	−0.05	−0.73	0.05	−0.58
29	5.46	5.4	0.42	0.90	0.17	0.70	0.12	−0.54	0.10	−0.46
30	4.51	4.32	0.01	0.36	−0.62	0.87	0.02	−0.49	−0.17	−1.07

[a] Abbreviations hERG/el-phys and hERG/binding denote potencies (pIC_{50}) of a compound at hERG in electrophysiological and binding experiments, respectively. Data presented in columns T623S, S624A, S624T, Y652A, Y652F, F656M, F656T, and F656W characterize differences between potencies of the compounds at wild-type hERG and at the corresponding hERG mutant, ($pIC_{50}^{wt\text{-}hERG} - pIC_{50}^{mutant}$), in electrophysiological experiments.

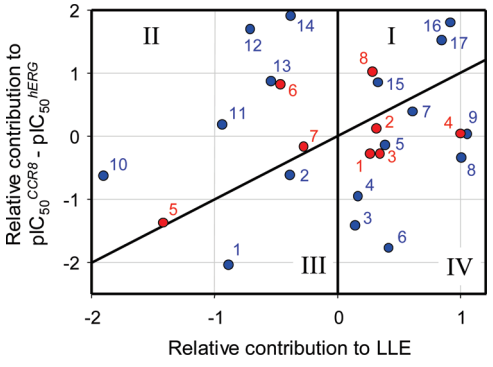

Figure 3. Results of fragment-based QSAR analysis of intrinsic interactions in the focused set of CCR8 antagonists with CCR8 and hERG obtained by Free−Wilson analysis performed in two directions, the LLE and the hERG selectivity, according to eq 3. Structures of the fragments are given in Figure 4. Fragments R1 are shown in blue, R2 in red. The nonorthogonal system of coordinates is made of the average lipophilicity baselines (the zero level of relative intrinsic potencies in the compound set) of hERG (the 45° diagonal line) and CCR8 (the vertical line) in binding assays. Fragments located below and above the diagonal axis are intrinsic hERG binding and intrinsic hERG nonbinding fragments, respectively. Fragments that appear to the left and to the right from the vertical axis are characteristic of promiscuous and direct attractive interactions with the primary target, respectively. Fragments that appear in the first quadrant of the coordinate system exhibit selective interactions with the primary target and, therefore, demonstrate the greatest potential for further optimization. The R1 fragment 17 was placed in the first quadrant according to its position obtained in the analogous plot that used hERG potency in the electrophysiological assay instead of hERG binding.

interactions with other off-target promiscuous binding sites, including metabolic enzymes and plasma proteins. Quadrants III and IV contain fragments that exhibit direct attractive interactions with the hERG ion channel and thereby are responsible for the unusually low hERG selectivity of the corresponding compounds. Fragments of the quadrants II and III reveal poor fit to the primary binding site and, thereby, the entire molecules have to have higher desolvation contribution to the intended potency to compensate the insufficient intrinsic complementarity with the primary binding site, which predisposes them to unwanted promiscuous interactions with target-unrelated binding sites.

The results of the QSAR analysis presented in Figures 3 and 4 reveal fragments that form selective interactions with CCR8. As is seen, fragments R2 at the right-hand side of the molecule (Figure 1) tend to move from the left to the right side of the plot in Figure 3 as soon as the number of polar heteroatoms increases, which indicates that the subsite of the CCR8 binding site they bind to is polar. They have to possess two polar functions that are able to form H-bonds with the CCR8 binding site to demonstrate a better than average contribution to LLE. Thus, 4-pyridine 7 is 14 times more efficient than *p*-Cl-phenyl 5 in direct interactions to the CCR8 binding site, which suggests that the 4-pyridine nitrogen makes an H-bond to CCR8. 2,4-Pyrimidine 2 is 4 times more efficient than 4-pyridine, therefore both nitrogens of fragment 2 are capable of H-bonding to CCR8. On the other hand, *N*-oxide-4-pyridine 3 is as efficient as 2,4-pyrimidine 2, which is likely to be caused by a stronger H-bonding capacity

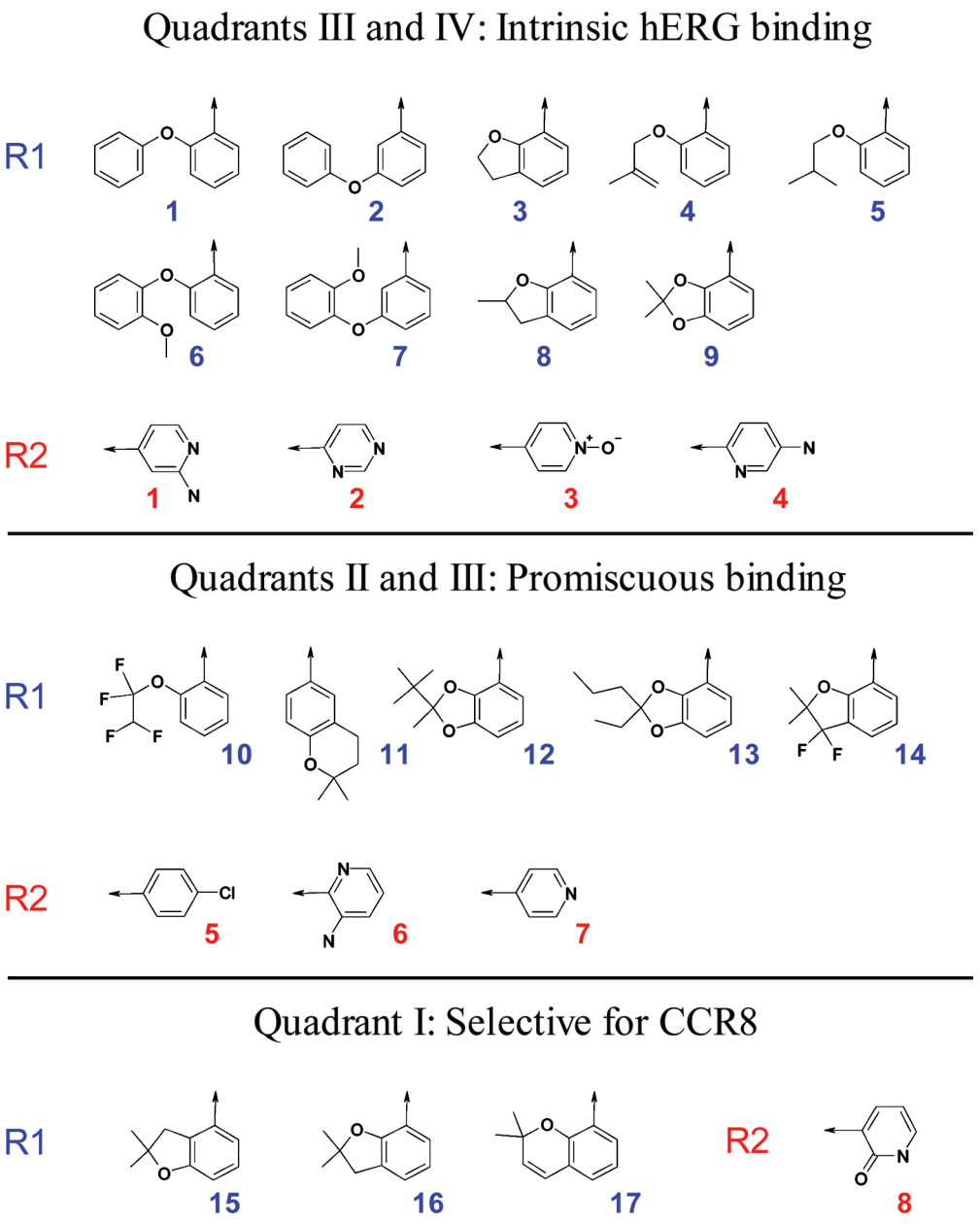

Figure 4. Structures of fragments of CCR8 antagonists of the focused set classified according to their potential for selective binding to the primary target as derived from the two-dimensional fragment-based QSAR analysis (Figure 3).

of the *N*-oxide-pyridine oxygen than the pyridine nitrogen. Surprisingly, replacement of any of the two H-bond acceptors in 2,4-pyrimidine 2 by a H-bond donor in fragments 1, 4, and 8 does not decrease stability of the H-bonding network with CCR8. This result is suggestive of flexibility of the polar subsite of the CCR8 binding site and possible involvement of residues Gln or Asn. Out of the five R2 fragments, 1−4 and 8, that demonstrate productive polar interactions with CCR8, fragments 4 and 8 stand out as most efficient in direct attractive interactions with CCR8 and direct repulsive interactions with hERG, respectively.

The structure of fragments R1 also dramatically affects LLE, but their efficiency in direct interactions with CCR8 is determined more by their geometric complementarity rather than their H-bonding capacity. Among the 10 R1 fragments that exhibit a better than average intrinsic binding to the CCR8 binding site, 3−9 and 15−17, there are fragments with one and two oxygens. However, the phenoxyphenyl oxygens in fragments 1, 2, 6, and 7 have been previously established to have no H-bonding capacity because of delocalization of their lone pairs in two benzene rings.[66] Results suggest that one of the oxygens capable of intermolecular H-bonding in R1 fragments is critical for efficient intrinsic interactions with the CCR8 binding site, but the second is not. This is the added first polar oxygen in the *ortho*-methoxy groups in fragments 6 and 7, which considerably improves otherwise poor values of LLE of 1 and 2. The second polar oxygen that exists in fragments 9, 12, and 13 does not further improves the LLE values, which are already achieved with the single oxygen in 8, 16, and 17. The position of the first polar oxygen in R1 is important for the binding efficiency. Thus, the ortho oxygen that exists in bicyclic fragments 8, 9, 16, and 17 is more efficient than the meta oxygen inherent in 15, whereas the only fragment with the *para* oxygen in the data set, 11, does not fit at all. These observations strongly suggest a single H-bonding capacity of the corresponding CCR8 subsite,

which implies that hydrophobic interactions and geometric complementarity are likely to be critical in this subsite.

The effects of methyl and short alkyl groups in bicyclic R1 fragments 8, 9, and 12−17 on the nondesolvation related interactions with the lipophilic subsite of CCR8 are remarkable. As is seen in Figure 3, the sole methyl group in fragment 8 increases the LLE of compounds by 0.9 logarithmic units (compare fragments 3 and 8), which indicates that this particular methyl group significantly improves geometric complementarity of compounds to the CCR8 binding site. It should be emphasized that this effect of the methyl group in 8 on LLE is something that comes in addition to the normally expected desolvation-driven contribution of 0.5 logarithmic units of a typical methyl group to compound potency.[47,67] It is well documented that in special cases small alkyl groups in bioactive compounds may cause unexpected "magic" effects on geometric complementarity or biological outcomes, effects that are far beyond their desolvation related interactions with biopolymers.[43,44,47,51,68−70] The dramatic effect of the sole methyl group in 8 on the nondesolvation related interactions with CCR8 allows us to regard this methyl as "magic". Surprisingly, the second methyl group in the bicyclic R1 fragments 9 and 15−17 does not add anything more to the LLE than is already achieved by the first methyl. The second methyl increases the CCR8 potency of compounds but adds just about as much to compound lipophilicity, thereby having a virtually zero effect on LLE, which is an indication of its purely desolvation-driven effects.

The dramatic effect of the "magic methyl" in R1 fragment 8 is especially surprising as this fragment is a mixture of two enantiomers. Our attempts to separate the enantiomers of the corresponding compound **19** failed. This may be because a chiral center located at the periphery of the molecule imparts little steric difference to the stereoisomers of **19**, which makes the separation virtually impossible. Normally only one of two enantiomers of bioactive compounds exhibits a special fit to the binding site, so the racemate is supposed to be less efficient than that particular enantiomer, which contradicts with the exceptional LLE-boosting performance of this "magic methyl". The results suggest that the single methyl in 8 is likely equally superior in both configurations. To shed light on this apparent discrepancy, we calculated the 3D structure of this fragment by fully optimized correlated ab initio calculations at the LMP2/cc-pVTZ(-f) level[71−73] using the program Jaguar 7.5 (Schrödinger, LLC). Calculations demonstrate that the dihydrofuran ring of 8 is not coplanar with the benzene ring and adopts an envelope conformation, with each of the stereoisomers having two equilibrium conformations of the same energy in which the "magic methyl" is in either equatorial or axial conformation. The results indicate that the 3D structures of the stereoisomers with the equatorial conformations of the "magic methyl" virtually coincide, whereas the structures with the axial conformations significantly differ. Figure 5 presents the overlaid 3D structures of the stereoisomers with the equatorial "magic methyls" by superposition of the benzene rings. Thus, we propose that the "magic methyl" of the R1 fragment 8 is equally efficient in boosting the stereochemical fit of compounds to the CCR8 binding site in both enantiomers being in the equatorial conformation.

The data presented in Figure 3 indicate that the R1 fragments 12−17 exhibit remarkable intrinsic anti-hERG

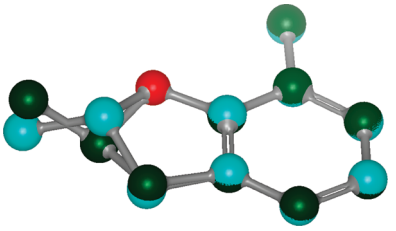

Figure 5. Superimposed structures of stereoisomers of the LLE-boosting R1 fragment 8 (Figure 4) with the single methyl being in the equatorial conformation obtained by ab initio calculations at the LMP2/cc-pVTZ(-f) level of theory. Carbons of the *S*- and *R*-enantiomers are shown in cyan and dark green, respectively. Hydrogens are not shown for clarity. Distance between carbon atoms of the methyl groups in the superimposed enantiomers is 0.78 Å.

propensities being well above the average hERG lipophilicity baseline. All these fragments contain a bicyclic ring system plus two small alkyl chains attached to the same carbon. As opposed to the less efficient R1 fragments 6 and 7, they have only one aromatic ring, which limits their potential for hydrophobic interactions with the channel and partially explains their lower contribution to hERG potency but does not explain their superior anti-hERG propensity given by eq 4. Note that the desolvation-driven components of potencies are virtually removed from the plot in Figure 3 so the fact that fragments 12−17 are separated from 6 and 7 by a hERG lipophilicity baseline is an indication that they lose much more in hERG potency than one would expect from their loss of lipophilicity. This extra drop in hERG potency contributions is due to their geometric incompatibility with the hERG channel cavity. These fragments also have significantly higher anti-hERG propensities than monocyclic fragments 4 and 5, which is linked to their conformational rigidity. The rigidity plus two alkyl chains at the periphery of the bicyclic system make fragments 12−17 very special in terms of anti-hERG propensity and set them apart from more flexible fragments 6 and 7 and also from ordinary bicyclic fragments 3 and 8. The presence of only one heteroatom capable of intermolecular H-bonding inherent in 12−17 is also an important feature, as the bicyclic fragment 9, which has two methyls but also two oxygens, is similar to 8 and nothing special in terms of the anti-hERG propensity. Thus, rigidity, bulkiness, and one polar heteroatom are the features that likely make these lipophilic left-hand side fragments of CCR8 antagonists significantly less predisposed for hERG binding than could be expected from their contribution to compound lipophilicity.

The roles the two peripheral alkyl groups in the bicyclic lipophilic fragments 12−17 play in hERG selectivity are different. As opposed to its effect on the intrinsic interactions with the primary target, the first "magic methyl" group does not contribute to the anti-hERG propensity because the line connecting the R1 fragments 3 (no methyls) and 8 (one methyl) in Figure 3 is about parallel to the hERG lipophilicity baseline. On the other hand, it is the second methyl, which is crucial for the anti-hERG propensity of the bicyclic R1 fragments, as is seen by comparing locations of R1 fragments 8 and 16 in the plot. Thus, both peripheral alkyl groups attached to the same sp^3-carbon in the bicyclic R1 fragments are "magic" contributors to the hERG selectivity of the CCR8 antagonists, with the first alkyl improving the geometric complementarity with the CCR8 binding site and

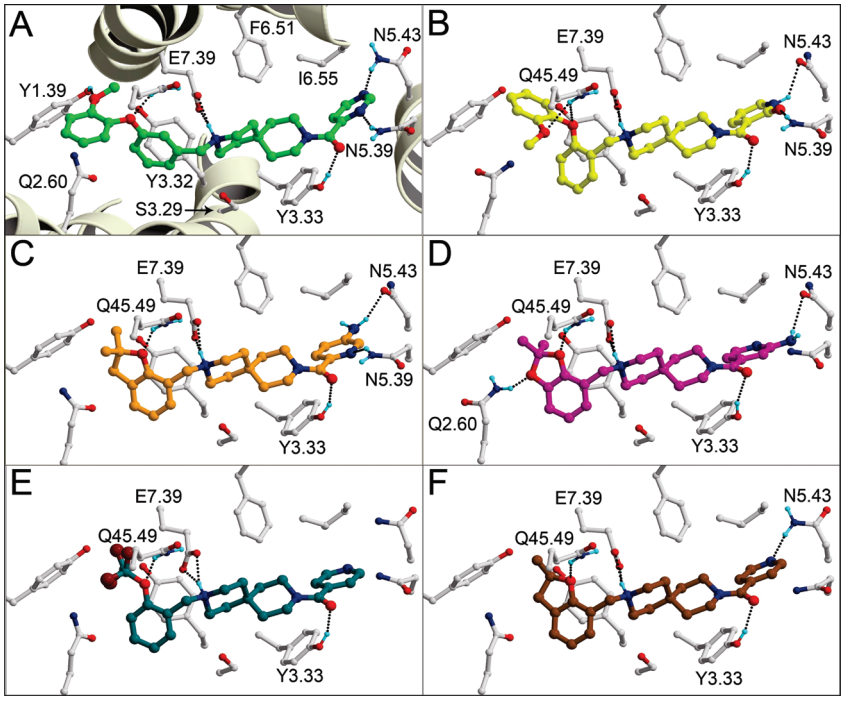

Figure 6. Refined docking poses selected by IFP of compounds **13** ((A) green carbon atoms), **16** ((B) yellow carbon atoms), **22** ((C) orange carbon atoms), **23** ((D) magenta carbon atoms), **7** ((E) dark-cyan carbon atoms), and the *R*-stereoisomer of **19** ((F) light-brown carbon atoms) in the CCR8 receptor. Parts of the backbone of TM helices 2, 3, 5, 6, and 7 are represented by light-yellow ribbons in (A). Important binding residues are depicted in a ball-and-stick fashion with gray carbon atoms. Oxygen, nitrogen, fluorine, and hydrogen atoms are colored red, blue, brown, and cyan, respectively. H-bonds described in the text are depicted by black dots.

the second alkyl causing steric clashes within the hERG pocket.

Only three lipophilic R1 fragments, 15, 16, and 17, and one polar R2 fragment, 8, are located in the first quadrant in Figure 3, which emphasizes their potential for further optimization. Although CCR8 represents the primary target, the overall success in the lead optimization campaign in increasing the LLE within this particular class is less impressive than the success in increasing their intrinsic anti-hERG propensity. As is seen in Figure 3, contributions of different fragments to the LLE in the focused set span 3.0 and 2.4 logarithmic units for R1 and R2 fragments, respectively, whereas their contributions to the anti-hERG propensity span correspondingly 4.3 and 2.1 logarithmic units. As a result, hERG selectivity in binding assays within the compound class span 6.3 logarithmic units, with about 2 logarithmic units being attributed to the discovery of the "magic" compact lipophilic bicyclic R1 fragments with the duo of two peripheral alkyl chains. This is the lipophilic periphery of the molecule, which seems to be the most efficient tool in removing hERG liability in the chemical class under investigation. The following site-directed mutagenesis studies of the hERG ion channel provide the structural explanation for high anti-hERG propensity of the distinct bicyclic lipophilic left-hand side fragments.

Structure-Based Rationalization of CCR8−Antagonist Interactions. CCR8 Binding Pocket and 3,9-Diazaspiro-[5.5]undecane Binding Mode. The proposed binding mode of the 3,9-diazaspiro[5.5]undecane scaffold to the CCR8 receptor model (Figure 6) is consistent with available experimental data. Like other chemokine receptors, CCR8 binds its ligands through the conserved glutamate residue $E^{7.39}$.[21,74−79] Site-directed mutagenesis of $Y^{1.39}$, $F^{2.57}$, $Q^{2.60}$, $S^{3.29}$, $Y^{3.32}$, $Y^{3.33}$, $F^{6.51}$, and $L^{6.55}$ to Ala indicated that they affect binding of nonpeptide ligands to CCR8.[21] Residues at corresponding positions in the closely related chemokine receptors CCR1 and CCR5 have been shown to be involved in antagonist binding.[74−79] Figure 6 shows the typical binding modes of 3,9-diazaspiro[5.5]undecanes automatically docked in the CCR8 homology model, in line with the reported site-directed mutagenesis studies and the structure−activity relationships presented in the present study. The protonated amine of the 3,9-diazaspiro[5.5]undecane scaffold forms a salt bridge with the negatively charged carboxylate group of $E^{7.39}$. Modification of this centrally located basic amine leads to a dramatic loss of CCR8 potency. Thus, the neutral *N*-oxide of **10** is 1.4 logarithmic units less potent than its positively charged parent compound. The amide oxygen of the scaffold forms an H-bond with the $Y^{3.33}$ hydroxyl group and in some compounds also with the hydroxyl group of $Y^{45.39}$ in the second extracellular loop. CCR8 antagonists occupy both subpockets i (TMs 1, 2, 3 and 7) and ii (TMs 3, 4, 5, 6), making aromatic interactions ($Y^{1.39}$, $Y^{3.32}$, and$Y^{3.33}$) and hydrophobic contacts ($M^{3.24}$, $Y^{45.51}$, $M^{5.43}$, $F^{6.51}$, and $L^{6.55}$) with the receptor. In our receptor model, residue $F^{2.57}$ does not directly interact with the antagonist but is a part of the aromatic cluster at the bottom of subpocket i ($Y^{1.39}$, $F^{2.53}$, $F^{2.57}$, $Y^{3.32}$, and $F^{7.43}$, not displayed in Figure 6 for reasons of clarity). Mutation of $S^{3.29}$ to a bulkier residue diminishes CCR8 agonist activity, while the smaller $S^{3.29}$A mutant shows comparable agonist activity as the wild-type receptor.[21] Increasing the size of this residue would interrupt the course of the narrow gorge between TM3 and TM7 in the receptor model and obstruct binding of the 3,9-diazaspiro[5.5]undecane scaffold (Figure 6).

Structure-Based Rationalization of Structure−Activity Relationships. The CCR8 homology model can satisfactorily rationalize the observed structure−activity relationships and

the results of the fragment-based QSAR analysis of CCR8 antagonists, which reveal polar interactions with the receptor binding site. The common spirocyclic core of the compound class (Figure 1) exhibits similar binding modes in different compounds docked to the receptor binding site and displays two direct attractive interactions, namely one ionic interaction of the basic amine with $E^{7.39}$ and one H-bond of the amide oxygen with $Y^{3.33}$. Consistent with the results of the QSAR analysis (Figure 3), the docking simulations show that the amide nitrogen atoms of $Q^{45.49}$ and $Q^{2.60}$, as well as the hydroxyl group of $Y^{1.39}$, can form hydrogen bonds with important polar oxygens in the lipophilic left-hand side (R1) of the antagonists in subpocket i. As is seen, the Asn residues that are able to be both H-bond donor and H-bond acceptor are indeed present in the polar subsite of the CCR8 TM pocket. The amide groups of $N^{5.39}$ and $N^{5.43}$ can form hydrogen bonds with both H-bond acceptors and donors of the polar right-hand side (R2) of the antagonists in subpocket ii. Figure 6 presents the binding modes of six docked antagonists and demonstrates how modifications in the R1 and R2 groups are reflected by the number and character of H-bond interactions between the antagonist and the CCR8 receptor. Table S2 of Supporting Information presents the H-bond interaction patterns with R1 and R2 groups of all 30 docked antagonists along with their LLE values.

Figure 6A,B shows how the methoxy oxygens of R1 fragments 7 (in compound **13**) and 6 (in compound **16**) accept one H-bond from residues $Y^{1.39}$ and $Q^{45.49}$, respectively. The phenoxyphenyl oxygen of fragments 1, 2, 6, and 7 are generally also within H-bond distance from $Q^{45.49}$ (Figure 6A,B, Table S2 of Supporting Information), but aromatic ether oxygen atoms are considered to have a poor H-bonding capacity,[66] which explains significantly lower contributions of R1 fragments 1 and 2 to LLE than those of fragments 3, 4, and 5 (see Figure 3). Alkoxy oxygen atoms in most other R1 fragments form H-bond interactions with $Q^{45.49}$ and/or $Q^{2.60}$ in the CCR8 receptor models as demonstrated for compounds **22** and **23** (Figure 6C,D) and reported in Table S2 of Supporting Information. Site-directed mutagenesis of $Q^{2.60}$ into a tryptophan residue (which is present in most other chemokine receptors[36] caused a significant decrease in the potency of CCR8 agonists,[21] supporting the involvement of this residue in ligand binding.

The H-bond acceptor and H-bond donor groups in the R2 fragments of antagonists can form one or more H-bonds in subpocket ii between TMs 3, 5, and 6. The H-bond acceptors positioned at the 2-position of the R2 ring generally form H-bonds with the amide nitrogen of $N^{5.39}$ (Figure 6A−C, Table S2 of Supporting Information), while H-bond acceptors or donors at the 3- and 4-positions can form H-bonds with the amide nitrogen or oxygen atoms of $N^{5.43}$ (Figure 6A−D,F and Table S2 of Supporting Information). This is in agreement with the fact that the LLE tends to increase with the increasing number as well as the H-bond capacity of heteroatoms in R2 (Figure 3). The *N*-oxide oxygen in R2 fragment 3 accepts one H-bond from $N^{5.43}$ but has a higher H-bonding capacity than the pyridine nitrogen in fragment 7, resulting in a higher LLE value (Figure 3). Fragments 2 (Figure 6A), 4 (Figure 6C), and 8 (Figure 6B) can form two H-bonds with $N^{5.39}$ and $N^{5.43}$ simultaneously (Table S2 of Supporting Information), explaining the relative increase in LLE when comparing compounds **4** and **5** or **8** and **10** (fragment 2 versus 7) and compounds **26** and **27** (fragment 4 versus 7). According to our docking simulations and in line with the results of the fragment-based QSAR analysis, R2 fragment 1 (Figure 6D) forms only one H-bond with the receptor binding site (compare compounds **25** and **26**), while the amine group of fragment 6 is ineffective because it only forms an intramolecular H-bond with the diazaspiro oxygen (compound **23** versus **24**). It should be noted, however, that water mediated contacts, as in the recently published crystal structure of the adenosine A_{2A} receptor,[5] are not taken into account in the present study.

Analysis of the binding mode of compound **7** suggests that the size and shape of the R1 fragment 10 might affect the binding orientation of the R2 group as the H-bond between the pyridine nitrogen in the ligand and the amide nitrogen of $N^{5.43}$ is disrupted for this compound (Figure 6E). Also in the complexes of compounds **12** and **15** with CCR8, the lipophilic R1 fragments, which possess a weak H-bonding capacity, disrupt H-bonding between their polar R2 fragments with $N^{5.43}$ (Table S2 of Supporting Information). The R1 fragments 3 and 11−14, however, are not predicted to affect the number of H-bond interactions between fragment R2 and the receptor (see compounds **17**−**18** and **28**−**30** in Table S2 of Supporting Information) while they have a negative relative contribution to LLE (Figure 3). Although more extensive computational efforts would be needed to accurately determine the geometric complementarity between R1 fragments and the receptor, the binding mode of compound **7** in Figure 6E suggests that highly bulky R1 fragments like 10−14 bump into the bottom of subpocket i between $Y^{1.39}$, $Q^{2.60}$, $Y^{3.32}$, and $E^{7.39}$. The R1 fragment 10, however, has by far the largest negative contribution to intrinsic CCR8 potency (Figure 3), and its binding is mainly driven by lipophilicity. The R1 fragment 3 in compound **20**, on the other hand, is probably too compact and therefore loosely bound (Figure 3), as it lacks the essential methyl group "anchor" of compound **19** (Figure 6F) to make hydrophobic and packing interactions in lipophilic subpocket i.

Site-Directed Mutagenesis of the hERG Channel. It is well documented that potency of hERG blockers within each compound class is linked to their lipophilicity.[26,80−83] Correspondingly, one normally has to expect an increase of hERG potency when adding lipophilic fragments to a hERG ion channel blocker (see eq 2). On the other hand, some distinct exceptions from this rule, when hERG potency remains unchanged or even decreased with the increase of compound lipophilicity within a structural class, have also been described.[43,44] It is important to identify the physical origin of the difference between these alternative effects of added lipophilicity on hERG potency. Both types of the effects of lipophilicity are present in the compound set (Tables 1, 2 and Table S1 of Supporting Information). The lipophilicity-driven increase of hERG potency is seen when comparing compounds **5** and **11**, **9** and **8**, **12** and **11**, **20** and **11**, **27** and **11**, or **26** and **29**, respectively. The alternative effect is illustrated by compound pairs **5** and **7**, **20** and **27**, **23** and **21**, **22** and **30**, or **29** and **28**, respectively. As is seen in Figure 3, lipophilic left-hand side fragments, 10−17, reveal significant intrinsic anti-hERG propensities. Lipophilic fragments 12 and 14 are most efficient to separate hERG binding from lipophilicity because they contribute to hERG binding more than 100 times less than it would be expected from the "average" left-hand side fragments in this compound series. To shed light on the alternative effects of

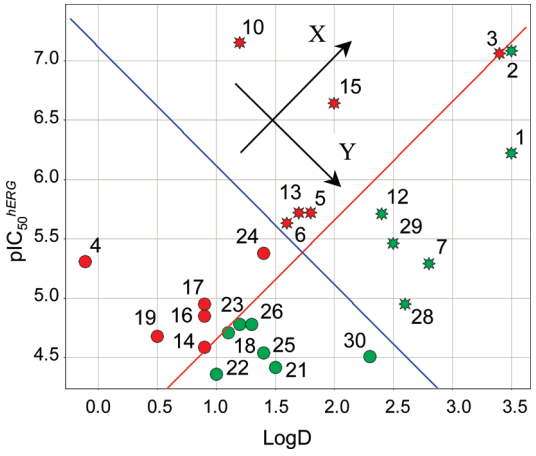

Figure 7. Plot of hERG potency in electrophysiological experiments versus measured compound lipophilicity for the subset of 25 CCR8 antagonists chosen for hERG site directed mutagenesis studies. The numbering of compounds is given in Table 1 and Table S1 of the Supporting Information. Two types of compound classifications are illustrated. The first classification, along the axes X, defined as ($pIC_{50}^{hERG} + Log\ D$), denotes the direction of the desolvation component of hERG potency. The second classification, along the axis Y, defined as $-(pIC_{50}^{hERG} - Log\ D)$, signifies repulsive nondesolvation related interactions with the hERG channel cavity (eq 4). The average blue line with the slope of -1 divides the compound set into two classes, hydrophobic (shown as stars) and polar (shown as spheres). The average red line with the slope of $+1$ splits the compound set into two classes of intrinsic hERG nonbinders (shown in green) and intrinsic hERG binders (shown in red). The following six compounds that cannot be unequivocally classified are excluded in the second classification: **2**, **3**, **14**, **18**, **23**, and **26**.

lipophilicity on hERG potency and, especially on the molecular mechanism of the anti-hERG propensity of the particular lipophilic fragments of CCR8 antagonists, electrophysiological measurements of eight hERG mutants have been performed using 25 compounds (Table 2). In each of these mutants, one of the residues that have been previously shown to be critical for binding of various hERG blockers, namely T623, S624, Y652, and F656,[84−87] was changed to make the following eight mutants of the channel: T623S, S624A, S624T, Y652A, Y652F, F656M, F656T, and F656W. The differences in potencies obtained at the wild-type hERG and the hERG mutants are presented in Table 2.

Figure 7 presents the plot of hERG potency of the 25 test compounds, which were chosen from the focused set, measured in electrophysiological experiments against their observed lipophilicity (Log $D_{7.4}$). A cross-validated PLS discriminant analysis (PLS-DA)[88] was applied to this compound set to understand the molecular basis for the two alternative effects of lipophilicity on hERG potency. Accordingly, two alternative classifications of this compound set were made. In the first classification, compounds were split into two classes along the axis X. In this particular classification, the compounds were grouped according to the sign of their contribution to the lipophilicity-driven component of hERG potency ($pIC_{50}^{hERG} + Log\ D$) with respect to its average value given by the blue line in Figure 7. Twelve compounds were classified as lipophilic hERG binders and the remaining 13 compounds as polar hERG binders. The PLS-DA was performed using the site-directed mutagenesis data (Table 2 and Table S1 of Supporting Information) as variables (SIMCA-P+ version 11; Umetrics, Kinnelon NJ).

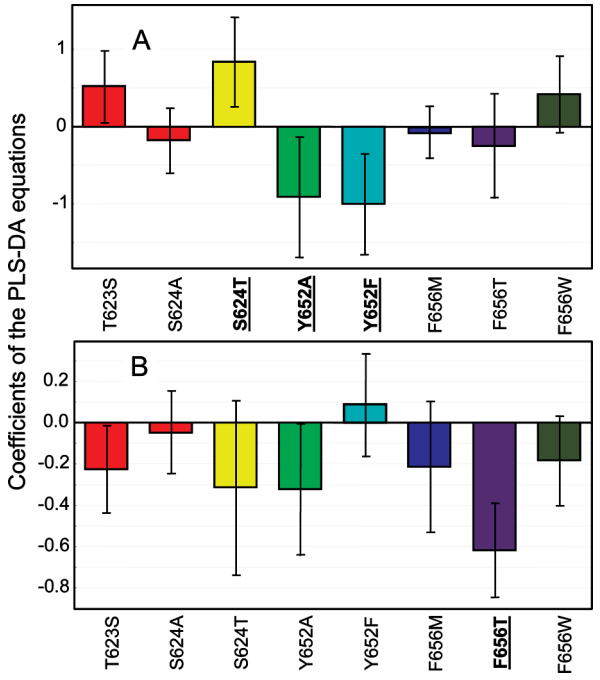

Figure 8. Results of two types of PLS-DA for different effects of added lipophilicity on hERG potency in electrophysiological assays in the subset of 25 CCR8 antagonists as described by the hERG site-directed mutagenesis data (Table 2 and Table S1 of the Supporting Information) as variables. Plot (A) describes the desolvation component of hERG potency; plot (B) describes repulsive nondesolvation related interactions within the hERG cavity. The coefficients of the optimal cross-validated PLS-DA linear equations are presented as histograms for hERG mutants T623S, S624A, S624T, Y652A, Y652F, F656M, F656T, and F656W. Positive coefficients indicate that compounds with added lipophilicity are more potent in the wild-type hERG than in the particular mutant with respect to the compounds of the alternative class. The error bars correspond to the confidence level of 95%. Highly significant coefficients are underlined.

The eight variables, i.e., the differences between potencies at wild-type hERG and at the particular mutants ($pIC_{50}^{wt\text{-}hERG} - pIC_{50}^{mutant}$), were centered but not scaled in order to take the magnitude of the observed effects of different mutations into account. This analysis helps to identify places in the hERG ion channel, where compounds of the different classes behave in the opposite ways. The cross-validated correlation coefficient obtained for this analysis was $q^2 = 0.48$. The coefficients of the optimal linear equation inherent in the more lipophilic class are presented in Figure 8A. A similar analysis was performed using the alternative classification of the set of compounds along axis Y in Figure 7, i.e., in the direction of the anti-hERG propensity given by eq 4. In this case, six compounds, namely **2**, **3**, **14**, **18**, **23**, and **26**, were excluded from classification as the corresponding data points were located too close to the average hERG lipophilicity baseline shown in red in Figure 7. Nine compounds with higher intrinsic anti-hERG propensities were classified as intrinsic hERG nonbinders, and the remaining 10 less lipophilic compounds as intrinsic hERG binders. The resulting PLS-DA showed the value of the cross-validated correlation coefficient of 0.34. The coefficients of the optimal linear equation characteristic of the more lipophilic class are presented in Figure 8B.

Coefficients of the PLS-DA equations shown in Figure 8 indicate where the two alternative types of added lipophilicity

in the compound set tend to interact with the hERG channel. A positive (or negative) coefficient of the PLS-DA equations indicates that the compounds with the added lipophilicity demonstrate a higher (or a lower) difference between potency at hERG and at the corresponding mutant than the less lipophilic compounds. As is seen in Figure 8A, the most significant feature that sets apart lipophilic and polar hERG binders is linked to the higher increase of potencies of compounds in the lipophilic class at mutants Y652A and Y652F than at the wild-type hERG channel and the higher increase of potencies at wild-type hERG than at the mutant S624T. In all of these three hERG mutants, Y652A, Y652F, and S624T, the lipophilicity-driven increase of potency is linked to the increase of the hERG channel vestibule size upon mutation. This suggests that the desolvation related component of hERG potency studied in the direction *X* (Figure 7) is associated with the added compound lipophilicity that fills the available space within the hERG channel vestibule. This result seems to disagree with the current opinion of the fundamental role of residues Y652 and F656 in hydrophobic interactions with hERG blockers.[42,84−87] However, the obtained data do not contradict with the importance of these key residues of the hERG cavity for binding of all known blockers. The PLS-DA focuses on what is different in the two classes but not on what is common. The origin of the appeared discrepancy can be understood by studying structural features of compounds that belong to the more lipophilic class along the desolvation component of hERG potency. Analysis of the 25 compounds that have been studied by site-directed mutagenesis suggests that the 2-phenoxyphenyl moiety dominates in this class. Four out of five compounds in the data set that possess this moiety, namely **2**, **3**, **10**, and **15**, belong to this class. This bulky moiety does not fit to the lower part of the hERG channel and likely fills the vestibule cavity,[44] which is in agreement with earlier studies that identified the ortho topology in hERG blockers as especially predisposed for hERG binding.[42] The lipophilic 2-phenoxyphenyl fragment needs a large room to be properly accommodated, correspondingly the more room that is available for this group in the channel vestibule, the higher the increase of potency is caused by the addition of this type of lipophilicity in the compound set, whether it is hERG or hERG mutant. On the other hand, most of the molecules of the less lipophilic class bind the hERG cavity in a classical way, in which the lipophilic periphery interacts with F656.[42] Accordingly, the PLS-DA detects that the lipophilicity-driven component of hERG potency in the particular data set is associated with filling the vestibule cavity. This result confirms our earlier predictions of positioning of the *ortho*-phenoxyphenyl peripheral moiety of CCR8 antagonists in the hERG vestibule.[44]

Within the second type of compound classification (Figure 8B), the most significant difference between the two classes is found to be in the F656T mutant. The negative value of the corresponding coefficient indicates that the more lipophilic class in the direction of the anti-hERG propensity (axis *Y* in Figure 7) demonstrates more difficulties in binding the wild-type hERG with respect to the F656T mutant than the less lipophilic class. Hydrophobic interactions of lipophilic peripheral fragments of hERG blockers with residue F656 in wild-type hERG are known to belong to the major determinants of their binding to the channel.[42,43,85,87,89] The F656T mutant is free of this determinant, as this mutant channel lacks four critical phenylalanine residues, and is much less hydrophobic at this place. Note that phenylalanine is roughly 1.4 logarithmic units more hydrophobic than threonine. Nevertheless, compounds **26**, **28**, **29**, and **30** of the more lipophilic class are roughly equipotent at the wild-type hERG and at the F656T mutant (Table 2). These are the first compounds ever reported that do not drop potency at the F656T mutant. In addition to the decrease in local lipophilicity, this particular place of the F656T mutant cavity displays more space available for blockers. The fact that compounds of the more lipophilic class demonstrate extra difficulties in binding the wild-type hERG but less problems with binding the F656T mutant suggests that the lipophilic peripheral fragments of these hERG blockers, which are supposed to bind to this particular narrow place in the funnel-looking hERG channel,[42] simply do not fit between the four residues F656 in hERG. Thus, the PLS-DA based on site-directed mutagenesis data and performed in the direction of the anti-hERG propensity in the particular data set suggests that the added lipophilicity does not fit to the hERG channel cavity in the region of residue F656.

The fact that the solution of the PLS-DA appears more blurry for the desolvation-driven component of hERG potency (Figure 8A) than for the anti-hERG propensity (Figure 8B) was expected. Desolvation-linked hydrophobic interactions of lipophilic compounds with lipophilic binding sites are nonspecific as they are virtually independent of the chemical nature of lipophilicity. Correspondingly, there are generally an abundance of lipophilic corners in binding sites and a vast variety of structural forms of lipophilic motifs in compounds, where these hydrophobic interactions can be exploited. On the other hand, the nondesolvation related direct interactions of compounds with binding sites are determined by stereochemical complementarity, which is highly dependent on structure. Whereas it is easier to increase compound potency by increasing lipophilicity, structural alterations leading to changes in the nondesolvation related interactions with binding sites, both intended and unintended, have more value in overcoming selectivity-related issues.

Results of the PLS-DA provide the interpretation for the observed geometric features of distinct lipophilic fragments of CCR8 antagonists that exhibit significant anti-hERG propensity. Figure 9 presents correlations of the relative anti-hERG propensity of a number of lipophilic left-hand side fragments of the CCR8 antagonists and their relative selectivity toward the F656T mutant versus the wild-type hERG ion channel. The plot was obtained by two-dimensional fragment-based QSAR analysis. The illustrated data suggest that the increase of the anti-hERG propensity of compounds caused by conformational rigidity and bulkiness of the distinct R1 fragments is indeed linked to difficulties in fitting compounds to the wild-type hERG with respect to the more spacious mutant F656T. As is seen, the preference of the two-oxygen R1 fragments 9, 13, and 12 for the F656T mutant does not increase as much as that of the one-oxygen fragments 5, 8, 16, 17, and 14. One possible explanation for this observation is that the mechanism of the anti-hERG propensity of the two-oxygen lipophilic R1 fragments involves multiple binding modes in the channel. In this case, bulky lipophilic fragments of this type could partially avoid clashes with the F656 residues of hERG channel by positioning in the vestibule cavity. Rigid bulky lipophilic peripheral

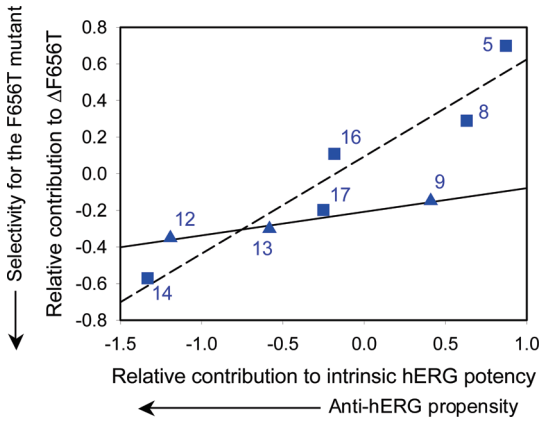

Figure 9. Correlations between anti-hERG propensity of lipophilic R1 fragments and their contribution to the selectivity of compounds for the F656T hERG mutant against the wild-type hERG. Axes *X* and *Y* are relative contributions of fragments to (pIC_{50}^{hERG} − Log *D*) and $\Delta F656T = (pIC_{50}^{wt\text{-}hERG} - pIC_{50}^{F656T\text{-}hERG})$, respectively, calculated by the Free−Wilson approach. Fragments are numbered according to Figure 4. Fragments with one oxygen are designated by squares, those with two oxygens by triangles. Linear regressions built separately on these two groups are illustrated.

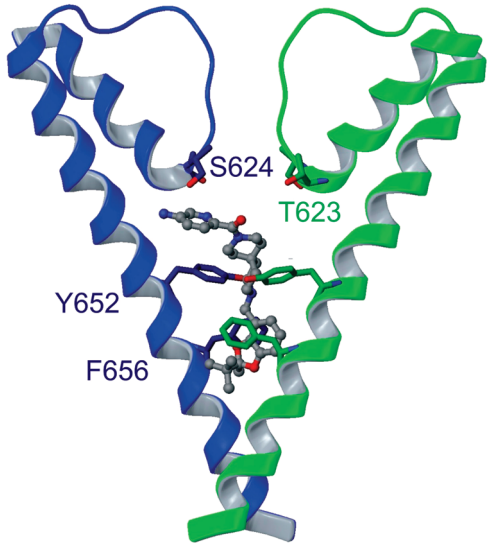

Figure 10. Interpretation of the intrinsic anti-hERG propensity of lipophilic peripheral fragments within the subset of CCR8 antagonists as it is seen from the results of hERG site directed mutagenesis. Only two of four subunits of the hERG channel are displayed for simplicity. Putative binding mode of compound **28** is illustrated; its bulky lipophilic group does not fit well to the hERG cavity in the space available between residues F656. The geometry of the channel was generated from a homology model of the closed hERG channel using the X-ray crystallographic structure of KcsA potassium ion channel (PDB entry 1R3J)[95] as it is described in ref 44. The residues that are known to be critical for binding of hERG ion channel blockers are illustrated.

fragments of CCR8 antagonists cause nondesolvation related repulsive interactions within the hERG ion channel cavity, thereby increasing selectivity against hERG because they do not fit to the space in the narrow part of the hERG channel between the four residues F656 but fit to the primary binding site. There are other narrow corners in the hERG channel that can be utilized for inducing direct repulsive interactions in particular structural classes by adding lipophilic groups. One of such corners, which is located in a vicinity of hERG pore helices, has been recently identified by site-directed mutagenesis studies using analogues of clofilium.[85]

The obtained results suggest a possible way of overcoming unintentional hERG binding when adding lipophilic fragments in chemical series. One should avoid lipophilic fragments that may fill the available space in the hERG ion channel cavity. Instead, one has to expand the lipophilic groups in the peripheral part of the molecules where they can cause steric clashes within the channel. Figure 10 gives a schematic representation of the direct repulsive interactions induced in the hERG channel by bulky lipophilic left-hand side fragment 12 in compound **28**. Consistent with the fragment-based QSAR studies, this is the second alkyl group in these fragments, which does not fit to the hERG channel cavity because the first alkyl likely avoids steric clashes with F656 by positioning along the channel axis in the equatorial conformation.

Conclusions

The increase of selectivity of biologically active compounds against undesirable binding to homologous proteins and various target-unrelated sites of interaction is very important in the lead optimization process. Most of the selectivity issues with respect to target-unrelated binding can be solved by increasing ligand lipophilicity efficiency (LLE) in the compound series. This is usually done by adding polar groups to a lead compound that form direct attractive interactions with the primary binding site. Apart from the important ionic interaction of the centrally located basic amine in CCR8 antagonists with $E^{7.39}$, we found four additional H-bonds that can be formed with CCR8, three of them associated with the polar subsite and one with the lipophilic subsite of the receptor.

When polarity of the lead compound is already at the higher limit, such that the further increase of polarity would jeopardize DMPK properties, the selectivity issues can alternatively be solved by adding lipophilic fragments to the molecules to induce direct repulsive interactions with the specific antitarget. In this report, we propose that the increase of bulkiness and rigidity of the lipophilic periphery of compounds in a series of CCR8 antagonists induces van der Waals clashes with F656 in the hERG ion channel. This residue forms the narrow part of the hERG ion channel, such that the bulky lipophilic peripheral moieties of the CCR8 antagonists do not fit. Site-directed mutagenesis studies of the hERG ion channel played a pivotal role in the interpretation of the observed anti-hERG propensity of distinct fragments of the CCR8 antagonists.

It is not easy to identify places in lipophilic binding sites of promiscuous antitargets like hERG, albumin, or metabolic enzymes, where lipophilic motifs of ligands can induce repulsive interactions, and the systematic investigation of nondesolvation related interactions with antitargets in a particular chemical class augmented by site-directed mutagenesis, is an effective pathway to detect these places. The emphasis on the nondesolvation related components of potencies, rather than on the overall affinities, illuminates structural features of molecules, which are important for selectivity and helps to develop compounds with enhanced safety margins, thereby increasing their chances to become drugs. This result is in line with previous studies that highlighted

the importance of nondesolvation related interactions for selectivity of drugs.[41,49]

Experimental Section

The potency of binding of the compounds under consideration to CCR8 was measured in the binding assay described in the literature.[22,90] The potency of binding to the hERG potassium ion channel was measured in an HEK cell line expressing recombinant hERG channel.[91,92] Measurements of compound lipophilicity, as described by the logarithm of the apparent *n*-octanol/water partition coefficient at pH = 7.4, Log $D_{7.4}$, are detailed in the literature.[93,94] Purity of compounds was determined to be more than 95% by HPLC with detection carried out at 220, 254, and 280 nm. For the electrophysiological measurements, an approach developed by Molecular Devices (Sunnyvale CA) that records averaged ionic currents from a population of cells expressing a recombinant hERG ion channel was utilized. Cells were plated into a 384-well PatchPlate substrate in which each well contained multiple recording sites, and the ionic currents were recorded using IonWorks HT medium-throughput electrophysiology device.

Acknowledgment. We gratefully acknowledge the support of many people at AstraZeneca R&D who have contributed to some aspects of the work presented in this paper. We thank Tim Hammond, Department of Safety Pharmacology, Safety Assessment UK, AstraZeneca R&D Alderley Park, for his sponsorship of electrophysiological studies of hERG mutants. We express our gratitude to Nicholas Tomkinson (AstraZeneca R&D Charnwood, UK) for writing a script for the QSAR analysis presented in the paper. C.d.G. gratefully acknowledges financial support from AstraZeneca R&D through a postdoctoral scholarship.

Supporting Information Available: Experimental procedures and characterization data for compounds **1**, **3**, **5**, **8**, **10**−**13**, **15**, **17**, **18**, **25**, and **28**−**30**. Full structures and experimental results obtained for the focused set of CCR8 antagonists as well as details of homology modeling and docking. This material is available free of charge via the Internet at http://pubs.acs.org.

References

(1) Gerard, C.; Rollins, B. J. Chemokines and disease. *Nat. Immunol.* **2001**, *2*, 108–115.
(2) Palczewski, K.; Kumasaka, T.; Hori, T.; Behnke, C. A.; Motoshima, H.; Fox, B. A.; Le Trong, I.; Teller, D. C.; Okada, T.; Stenkamp, R. E.; Yamamoto, M.; Miyano, M. Crystal structure of rhodopsin: A G-protein-coupled receptor. *Science* **2000**, *289*, 739–745.
(3) Cherezov, V.; Rosenbaum, D. M.; Hanson, M. A.; Rasmussen, S. G.; Thian, F. S.; Kobilka, T. S.; Choi, H. J.; Kuhn, P.; Weis, W. I.; Kobilka, B. K.; Stevens, R. C. High-resolution crystal structure of an engineered human beta2-adrenergic G protein-coupled receptor. *Science* **2007**, *318*, 1258–1265.
(4) Warne, T.; Serrano-Vega, M. J.; Baker, J. G.; Moukhametzianov, R.; Edwards, P. C.; Henderson, R.; Leslie, A. G.; Tate, C. G.; Schertler, G. F. Structure of a β_1-adrenergic G-protein-coupled receptor. *Nature* **2008**, *454*, 486–491.
(5) Jaakola, V. P.; Griffith, M. T.; Hanson, M. A.; Cherezov, V.; Chien, E. Y.; Lane, J. R.; Ijzerman, A. P.; Stevens, R. C. The 2.6 angstrom crystal atructure of a human A_{2A} adenosine receptor bound to an antagonist. *Science* **2008**, *322*, 1211–1217.
(6) Ballesteros, J.; Palczewski, K. G-protein-coupled receptor drug discovery: implications from crystal structure of rhodopsin. *Curr. Opin. Drug Discovery Dev.* **2001**, *4*, 561–574.
(7) Ballesteros, J. A.; Shi, L.; Javitch, J. A. Structural mimicry in G-protein-coupled receptors: implications of the high-resolution structure of rhodopsin for structure-function analysis of rhodopsin-like receptors. *Mol. Pharmacol.* **2001**, *60*, 1–19.
(8) de Graaf, C.; Rognan, D. Customizing G-protein-coupled receptor models for structure-based virtual screening. *Curr. Pharm. Des.* **2009**, in press.
(9) Deupi, X.; Dölker, N.; López-Rodríguez, M. L.; Campillo, M.; Ballesteros, J. A.; Pardo, L. Structural models of class A G-protein-coupled receptors as a tool for drug design: insights on transmembrane bundle plasticity. *Curr. Top. Med. Chem.* **2007**, *7*, 991–998.
(10) Qu, C.; Edwards, E. W.; Tacke, F.; Angeli, V.; Llodrá, J.; Sanchez-Schmitz, G.; Garin, A.; Haque, N. S.; Peters, W.; van Rooijen, N.; Sanchez-Torres, C.; Bromberg, J.; Charo, I. F.; Jung, S.; Lira, S. A.; Randolph, G. J. Role of CCR8 and other chemokine pathways in the migration of monocyte-derived dendritic cells to lymph nodes. *J. Exp. Med.* **2004**, *200*, 1231–1241.
(11) Soler, D.; Chapman, T. R.; Poisson, L. R.; Wang, L.; Cote-Sierra, J.; Ryan, M.; McDonald, A.; Badola, S.; Fedyk, E.; Coyle, A. J.; Hodge, M. R.; Kolbeck, R. CCR8 Expression identifies CD4 memory T cells enriched for FOXP3+ regulatory and Th2 effector lymphocytes. *J. Immunol.* **2006**, *177*, 6940–6951.
(12) Panina-Bordignon, P.; Papi, A.; Mariani, M.; Di Lucia, P.; Casoni, G.; Bellettato, C.; Buonsanti, C.; Miotto, D.; Mapp, C.; Villa, A.; Arrigoni, G.; Fabbri, L. M.; Sinigaglia, F. The C−C chemokine receptors CCR4 and CCR8 identify airway T cells of allergen-challenged atopic asthmatics. *J. Clin. Invest.* **2001**, *107*, 1357–1364.
(13) Sebastiani, S.; Albanesi, C.; De Pità, O.; Puddu, P.; Cavani, A.; Girolomoni, G. The role of chemokines in allergic contact dermatitis. *Arch. Dermatol. Res.* **2002**, *293*, 552–559.
(14) Peroni, D. G.; Panina-Bordignon, P.; Piacentini, G. L.; Bodini, A.; Ress, M.; Mariani, M.; Sinigaglia, F.; Boner, A. L. CC chemokine receptor expression in childhood asthma is influenced by natural allergen exposure. *Pediatr. Allergy Immunol.* **2006**, *17*, 495–500.
(15) Chensue, S. W.; Lukacs, N. W.; Yang, T. Y.; Shang, X.; Frait, K. A.; Kunkel, S. L.; Kung, T.; Wiekowski, M. T.; Hedrick, J. A.; Cook, D. N.; Zingoni, A.; Narula, S. K.; Zlotnik, A.; Barrat, F. J.; O'Garra, A.; Napolitano, M.; Lira, S. A. Aberrant in vivo T helper type 2 cell response and impaired eosinophil recruitment in CC chemokine receptor 8 knockout mice. *J. Exp. Med.* **2001**, *193*, 573–584.
(16) Buckland, K. F.; O'Connor, E. C.; Coleman, E. M.; Lira, S. A.; Lukacs, N. W.; Hogaboam, C. M. Remission of chronic fungal asthma in the absence of CCR8. *J. Allergy Clin. Immunol.* **2007**, *119*, 997–1004.
(17) Norman, P. CCR8 antagonists. *Expert Opin. Ther. Patents* **2007**, *17*, 465–469.
(18) Pease, J. E.; Horuk, R. Chemokine receptor antagonists: Part 2. *Expert Opin. Ther. Patents* **2009**, *19*, 199–221.
(19) Pease, J. E.; Horuk, R. Chemokine receptor antagonists: Part 1. *Expert Opin. Ther. Patents* **2009**, *19*, 39–58.
(20) Dragic, T.; Trkola, A.; Thompson, D. A. D.; Cormier, E. G.; Kajumo, F. A.; Maxwell, E.; Lin, S. W.; Ying, W.; Smith, S. O.; Sakmar, T. P.; Moore, J. P. A binding pocket for a small molecule inhibitor of HIV-1 entry within the transmembrane helices of CCR5. *Proc. Natl. Acad. Sci. U.S.A.* **2000**, *97*, 5639–5644.
(21) Jensen, P. C.; Nygaard, R.; Thiele, S.; Elder, A.; Zhu, G.; Kolbeck, R.; Ghosh, S.; Schwartz, T. W.; Rosenkilde, M. M. Molecular interaction of a potent nonpeptide agonist with the chemokine receptor CCR8. *Mol. Pharmacol.* **2007**, *72*, 327–340.
(22) (a) Bladh, H.; Connolly, S.; Dyke, H. J.; Lisius, A.; Price, S.; Shamovsky, I.; van den Heuvel, M. Preparation of novel diazaspiroalkanes and their use for treatment of chemokine receptor CCR8 mediated diseases. PCT Int. Appl. WO2005040167, **2005**, 136 pp. (b) Connolly, S.; Skrinjar, M. Novel diazaspiroalkanes and their use for treatment of CCR8 mediated diseases. PCT Int. Appl. WO2006107252, **2006**, 47 pp. (c) Connolly, S.; Linnanen, T.; Skrinjar, M. Novel diazaspiroalkanes and their use for treatment of CCR8 mediated diseases. PCT Int. Appl. WO2006107253, **2006**, 55 pp. (d) Connolly, S.; Skrinjar, M. Novel diazaspiroalkanes and their use for treatment of CCR8 mediated diseases. PCT Int. Appl. WO2006107254, **2006**, 44 pp. (e) Börjesson, L.; Connolly, S.; Johansson, H.; Kristoffersson, A.; Linnanen, T.; Shamovsky, I.; Skrinjar, M. Preparation of novel diazaspiroalkanes for treatment of CCR8 mediated diseases. PCT Int. Appl. WO2007030061, **2007**, 257 pp.
(23) Jin, J.; Wang, Y.; Wang, F.; Kerns, J. K.; Vinader, V. M.; Hancock, A. P.; Lindon, M. J.; Stevenson, G. I.; Morrow, D. M.; Rao, P.; Nguyen, C.; Barrett, V. J.; Browning, C.; Hartmann, G.; Andrew, D. P.; Sarau, H. M.; Foley, J. J.; Jurewicz, A. J.; Fornwald, J. A.; Harker, A. J.; Moore, M. L.; Rivero, R. A.; Belmonte, K. E.; Connor, H. E. Oxazolidinones as novel human CCR8 antagonists. *Bioorg. Med. Chem. Lett.* **2007**, *17*, 1722–1725.
(24) Jenkins, T. J.; Guan, B.; Dai, M.; Li, G.; Lightburn, T. E.; Huang, S.; Freeze, B. S.; Burdi, D. F.; Jacutin-Porte, S.; Bennett, R.; Chen, W.; Minor, C.; Ghosh, S.; Blackburn, C.; Gigstad, K. M.; Jones, M.; Kolbeck, R.; Yin, W.; Smith, S.; Cardillo, D.; Ocain, T. D.; Harriman, G. C. Design, synthesis, and evaluation of naphthalenesulfonamide antagonists of human CCR8. *J. Med. Chem.* **2007**, *50*, 566–584.

(25) Morgan, T. K., Jr.; Sullivan, M .E. An overview of Class III electrophysiological agents: a new generation of antiarrhythmic therapy. *Prog. Med. Chem.* **1992**, *29*, 65–108.
(26) Aronov, A. M. Ligand structural aspects of hERG channel blockade. *Curr. Top. Med. Chem.* **2008**, *8*, 1113–1127.
(27) Wang, X.-J.; Yang, Q.; Yin, D.-L.; Chen, Y.-D.; You, Q.-D. A pharmacophore modeling study of drugs inducing cardiotoxic side effects. *Chin. J. Chem.* **2008**, *26*, 2125–2132.
(28) de Graaf, C.; Vermeulen, N. P.; Feenstra, K. A. Cytochrome P450 in silico: an integrative modeling approach. *J. Med. Chem.* **2005**, *48*, 2725–2755.
(29) Westby, M.; van der Ryst, E. CCR5 antagonists: host-targeted antivirals for the treatment of HIV infection. *Antiviral Chem. Chemother.* **2005**, *16*, 339–354.
(30) Horuk, R. BX471: A CCR1 antagonist with anti-inflammatory activity in man. *Mini-Rev. Med. Chem.* **2005**, *5*, 791–804.
(31) Fox, D. J.; Reckless, J.; Wilbert, S. M.; Greig, I.; Warren, S.; David, J.; Grainger, D. J. Identification of 3-(acylamino)azepan-2-ones as stable broad-spectrum chemokine inhibitors resistant to metabolism in vivo. *J. Med. Chem.* **2005**, *48*, 867–874.
(32) De Lucca, G. V. Recent developments in CCR3 antagonists. *Curr. Opin. Drug Discovery Dev.* **2006**, *9*, 516–524.
(33) Purandare, A. V.; Wan, H.; Somerville, J. E.; Burke, C.; Vaccaro, W.; Yang, X.; McIntyre, K. W.; Poss, M. A. Core exploration in optimization of chemokine receptor CCR4 antagonists. *Bioorg. Med. Chem. Lett.* **2007**, *17*, 679–682.
(34) Sato, I.; Morihira, K.; Inami, H.; Kubota, H.; Morokata, T.; Suzuki, K.; Iura, Y.; Nitta, A.; Imaoka, T.; Takahashi, T.; Takeuchi, M.; Ohta, M.; Tsukamoto, S. Design and synthesis of 6-fluoro-2-naphthyl derivatives as novel CCR3 antagonists with reduced Cyp2D6 inhibition. *Bioorg. Med. Chem.* **2008**, *16*, 8607–8618.
(35) Leeson, P. D.; Springthorpe, B. The influence of drug-like concepts on decision-making in medicinal chemistry. *Nat. Drug Discovery* **2007**, *6*, 881–890.
(36) Surgand, J. S.; Rodrigo, J.; Kellenberger, E.; Rognan, D. A chemogenomic analysis of the transmembrane binding cavity of human G-protein-coupled receptors. *Proteins* **2006**, *62*, 509–538.
(37) Lewis, D. F. V.; Dickins, M. Baseline lipophilicity relationships in human cytochromes P450 associated with drug metabolism. *Drug Metab. Rev.* **2003**, *35*, 1–18.
(38) Lewis, D. F. V. Quantitative structure−activity relationships (QSARs) for substrates of human cytochromes P450 CYP2 family enzymes. *Toxicol. In Vitro* **2004**, *18*, 89–97.
(39) Lewis, D. F. V. Hydrogen bonding in human P450−substrate interactions: a major contribution to binding affinity. *The Scientific World* **2004**, *4*, 1074–1082.
(40) Lewis, D. F. V.; Jacobs, M. N.; Dickins, M. Compound lipophilicity for substructure binding to human P450s in drug metabolism. *Drug Discovery Today* **2004**, *9*, 530–537.
(41) Ruben, A. J.; Kiso, Y.; Freire, E. Overcoming roadblocks in lead optimization: a thermodynamic perspective. *Chem. Biol. Drug Des.* **2006**, *67*, 2–4.
(42) Aronov, A. M. Predictive in silico modeling for hERG channel blockers. *Drug Discovery Today* **2005**, *10*, 149–155.
(43) Jamieson, C.; Moir, E. M.; Rankovic, Z.; Wishart, G. Medicinal chemistry of hERG optimizations: highlights and hang-ups. *J. Med. Chem.* **2006**, *49*, 5029–5046.
(44) Shamovsky, I. L.; Connolly, S.; David, L.; Ivanova, S.; Nordén, B.; Springthorpe, B.; Urbahns, K. Overcoming undesirable hERG potency of chemokine receptor antagonists using baseline lipophilicity relationships. *J. Med. Chem.* **2008**, *51*, 1162–1178.
(45) Kubinyi, H. Lipophilicity and drug activity. *Prog. Drug. Res.* **1979**, *23*, 97–198.
(46) Lewis, D. F. V.; Lake, B. G.; Dickins, M. Quantitative structure−activity relationships (QSARs) in inhibitors of various cytochromes P450: The importance of compound lipophilicity. *J. Enzyme Inhib. Med. Chem.* **2007**, *22*, 1–6.
(47) Davis, A. M.; Teague, S. J. Hydrogen bonding, hydrophobic interactions, and failure of the rigid receptor hypothesis. *Angew. Chem., Int. Ed.* **1999**, *38*, 736–749.
(48) DeLano, W. L.; Ultsch, M. H.; de Vos, A. M.; Wells, J. A. Convergent solutions to binding at a protein−protein interface. *Science* **2000**, *287*, 1279–1283.
(49) Davis, A. M.; Dixon, J.; Logan, C. J.; Payling, D. W. Accelerating the progress of drug discovery. In *Pharmacokinetic Challenges in Drug Discovery*; Pelkonen, O., Baumann, A., Reichel, A., Eds.; Springer: New York, 2002; pp 1−32, E. Schering Research Foundation, Workshop 37 .
(50) de Graaf, C.; Foata, N.; Engkvist, O.; Rognan, D. Molecular modeling of the second extracellular loop of G-protein-coupled receptors and its implication on structure-based virtual screening. *Proteins* **2008**, *71*, 599–620.
(51) Kellenberger, E.; Springael, J. Y.; Parmentier, M.; Hachet-Haas, M.; Galzi, J. L.; Rognan, D. Identification of nonpeptide CCR5 receptor agonists by structure-based virtual screening. *J. Med. Chem.* **2007**, *50*, 1294–1303.
(52) Bissantz, C.; Logean, A.; Rognan, D. High-throughput modeling of human G-protein-coupled receptors: amino acid sequence alignment, three-dimensional model building, and receptor library screening. *J. Chem. Inf. Comput. Sci.* **2004**, *44*, 1162–1176.
(53) Ballesteros, J. A.; Weinstein, H. Integrated methods for the construction of three-dimensional models and computational probing of structure-function relations in G-protein-coupled receptors. *Methods Neurosci.* **1995**, *25*, 366–428.
(54) Brady, G. P.; Pieter, F. W. S. Fast prediction and visualization of protein binding pockets with PASS. *J. Comput.-Aided Mol. Des.* **2000**, *14*, 383–401.
(55) de Graaf, C.; Rognan, D. Selective structure-based virtual screening for full and partial agonists of the β_2 adrenergic receptor. *J. Med. Chem.* **2008**, *51*, 4978–4985.
(56) Marcou, G.; Rognan, D. Optimizing fragment and scaffold docking by use of molecular interaction fingerprints. *J. Chem. Inf. Model.* **2007**, *47*, 195–207.
(57) Schroeder, K.; Neagle, B.; Trezise, D. J.; Worley, J.; IonWorks, H. T. A new high-throughput electrophysiology measurement platform. *J. Biomol. Screen.* **2003**, *8*, 50–64.
(58) Bridgland-Taylor, M. H.; Hargreaves, A. C.; Easter, A.; Orme, A.; Henthorn, D. C.; Ding, M.; Davis, A. M.; Small, B. G.; Heapy, C. G.; Abi-Gerges, N.; Persson, F.; Jacobson, I.; Sullivan, M.; Albertson, N.; Hammond, T. G.; Sullivan, E.; Valentin, J. P.; Pollard, C. E. Optimization and validation of a medium-throughput electrophysiology-based hERG assay using IonWorks HT. *J. Pharmacol. Toxicol. Methods* **2006**, *54*, 189–199.
(59) Obach, R. S.; Lombardo, F.; Waters, N. J. Trend analysis of a database of intravenous pharmacokinetic parameters of humans for 670 drug compounds. *Drug Metab. Dispos.* **2008**, *36*, 1385–1405.
(60) Hughes, J. D.; Blagg, J.; Price, D. A.; Bailey, S.; DeCrescenzo, G. A.; Devraj, R. V.; Ellsworth, E.; Fobian, Y. M.; Gibbs, M. E.; Gilles, R. W.; Greene, N.; Huang, E.; Krieger-Burke, T.; Loesel, J.; Wager, T.; Whiteley, L.; Zhang, Y. Physiochemical drug properties associated with in vivo toxicological outcomes. *Bioorg. Med. Chem. Lett.* **2008**, *18*, 4872–4875.
(61) Dey, A.; Okamura, T.; Ueyama, N.; Hedman, B.; Hodgson, K. O.; Solomon, E. I. Sulfur K-edge XAS and DFT calculations on P450 model complexes: effects of hydrogen bonding on electronic structure and redox potentials. *J. Am. Chem. Soc.* **2005**, *127*, 12046–12053.
(62) Lewis, D. F. V.; Lake, B. G.; Ito, Y.; Dickins, M. Lipophilicity relationships in inhibitors of CYP2C9 and CYP2C19 enzymes. *J. Enzyme Inhib. Med. Chem.* **2006**, *21*, 385–389.
(63) de Graaf, C.; Oostenbrink, C.; Keizers, P. H. J.; van Vugt-Lussenburg, B. M. A.; Commandeur, J. N. M.; Vermeulen, N. P. E. Free energies of binding of *R*- and *S*-propranolol to wild-type and F483A mutant cytochrome P450-2D6 from molecular dynamics simulations. *Eur. Biophys. J.* **2007**, *36*, 589–599.
(64) Franklin, T. J.; Jacobs, V. N.; Jones, G.; Ple, P. Human colorectal carcinoma cells in vitro as a means to assess the metabolism of analogs of mycophenolic acid. *Drug Metab. Dispos.* **1997**, *25*, 367–370.
(65) Free, S. M., Jr.; Wilson, J. W. A mathematical contribution to structure−activity studies. *J. Med. Chem.* **1964**, *7*, 395–399.
(66) Kubinyi, H. Hydrogen bonding, the last mystery in drug design? In *Pharmacokinetic Optimization in Drug Research. Biological, Physicochemical, and Computational Strategies*; Testa, B., van de Waterbeemd, H., Folkers, G., Guy, R., , Eds.; Helvetica Chimica Acta and Wiley-VCH: Zurich, 2001, pp. 513−524.
(67) Ferguson, J. The use of chemical potentials as indices of toxicity. *Proc. R. Soc. London, Ser. B* **1939**, *127*, 387–404.
(68) Bigge, C. F.; Nikam, S. S. AMPA receptor agonists, antagonists and modulators: their potential for clinical utility. *Exp. Opin. Ther. Patents* **1997**, *7*, 1099–1114.
(69) Zhi, L.; Tegley, C. M.; Marschke, K. B.; Jones, T. K. Switching androgen receptor antagonists to agonists by modifying C-ring substituents on piperidino[3,2-*g*] quinolinone. *Bioorg. Med. Chem. Lett.* **1999**, *9*, 1009–1012.
(70) De Lucca, G. V.; Kim, U. T.; Johnson, C.; Vargo, B. J.; Welch, P. K.; Covington, M.; Davies, P.; Solomon, K. A.; Newton, R. C.; Trainor, G. L.; Decicco, C. P.; Ko, S. S. Discovery and structure−activity relationship of *N*-(ureidoalkyl)-benzyl-piperidines as potent small molecule CC chemokine receptor-3 (CCR3) antagonists. *J. Med. Chem.* **2002**, *45*, 3794–3804.
(71) Møller, C.; Plesset, M. S. Note on an approximation treatment for many-electron systems. *Phys. Rev.* **1934**, *46*, 618–622.

(72) Sæbø, S.; Pulay, P. Local treatment of electron correlation. *Annu. Rev. Phys. Chem.* **1993**, *44*, 213–236.
(73) Sæbø, S.; Tong, W.; Pulay, P. Efficient elimination of basis-set-superposition errors by the local correlation method: accurate ab initio studies of the water dimer. *J. Chem. Phys.* **1993**, *98*, 2170–2175.
(74) Castonguay, L. A.; Weng, Y.; Adolfsen, W.; Di Salvo, J.; Kilburn, R.; Caldwell, C. G.; Daugherty, B. L.; Finke, P. E.; Hale, J. J.; Lynch, C. L.; Mills, S. G.; MacCoss, M.; Springer, M. S.; DeMartino, J. A. Binding of 2-aryl-4-(piperidin-1-yl)butanamines and 1,3,4-trisubstituted pyrrolidines to human CCR5: a molecular modeling-guided mutagenesis study of the binding pocket. *Biochemistry* **2003**, *42*, 1544–1550.
(75) Tsamis, F.; Gavrilov, S.; Kajumo, F.; Seibert, C.; Kuhmann, S.; Ketas, T.; Trkola, A.; Palani, A.; Clader, J. W.; Tagat, J. R.; McCombie, S.; Baroudy, B.; Moore, J. P.; Sakmar, T. P.; Dragic, T. Analysis of the mechanism by which the small-molecule CCR5 antagonists SCH-351125 and SCH-350581 inhibit human immunodeficiency virus type 1 entry. *J. Virol.* **2003**, *77*, 5201–5208.
(76) de Mendonca, F .L.; da Fonseca, P. C.; Phillips, R. M.; Saldanha, J. W.; Williams, T. J.; Pease, J. E. Site-directed mutagenesis of CC chemokine receptor 1 reveals the mechanism of action of UCB 35625, a small molecule chemokine receptor antagonist. *J. Biol. Chem.* **2005**, *280*, 4808–4816.
(77) Seibert, C.; Ying, W.; Gavrilov, S.; Tsamis, F.; Kuhmann, S. E.; Palani, A.; Tagat, J. R.; Clader, J. W.; McCombie, S. W.; Baroudy, B. M.; Smith, S. O.; Dragic, T.; Moore, J. P.; Sakmar, T. P. Interaction of small molecule inhibitors of HIV-1 entry with CCR5. *Virology* **2006**, *349*, 41–54.
(78) Maeda, K.; Das, D.; Ogata-Aoki, H.; Nakata, H.; Miyakawa, T.; Tojo, Y.; Norman, R.; Takaoka, Y.; Ding, J.; Arnold, G. F; Arnold, E.; Mitsuya, H. Structural and molecular interactions of CCR5 inhibitors with CCR5. *J. Biol. Chem.* **2006**, *281*, 12688–12698.
(79) Vaidehi, N.; Schlyer, S.; Trabanino, R. J.; Floriano, W. B.; Abrol, R.; Sharma, S.; Kochanny, M.; Koovakat, S.; Dunning, L.; Liang, M.; Fox, J. M.; de Mendonca, F. L.; Pease, J. E.; Goddard, W. A., III; Horuk, R. Predictions of CCR1 chemokine receptor structure and BX 471 antagonist binding followed by experimental validation. *J. Biol. Chem.* **2006**, *281*, 27613–27620.
(80) Pearlstein, R. A.; Vaz, R. J.; Kang, J.; Chen, X.-L.; Preobrazhenskaya, M.; Shchekotikhin, A. E.; Korolev, A. M.; Lysenkova, L. N.; Miroshnikova, O. V.; Hendrix, J.; Rampe, D. Characterization of HERG potassium channel inhibition using CoMSiA 3D QSAR and homology modelling approaches. *Bioorg. Med. Chem. Lett.* **2003**, *13*, 1829–1835.
(81) Aronov, A. M.; Goldman, B. B. A model for identifying hERG K+ channel blockers. *Bioorg. Med. Chem.* **2004**, *12*, 2307–2315.
(82) Recanatini, M.; Poluzzi, E.; Masetti, M.; Cavalli, A.; De Ponti, F. QT prolongation through hERG K+ channel blockade: current knowledge and strategies for the early prediction during drug development. *Med. Res. Rev.* **2005**, *25*, 133–166.
(83) Waring, M. J.; Johnstone, C. A quantitative assessment of hERG liability as a function of lipophilicity. *Bioorg. Med. Chem. Lett.* **2007**, *17*, 1759–1764.
(84) Fernandez, D.; Ghanta, A.; Kauffman, G. W.; Sanguinetti, M. C. Physicochemical features of the hERG channel drug binding site. *J. Biol. Chem.* **2004**, *279*, 10120–10127.
(85) Perry, M.; Stansfeld, P. J.; Leaney, J.; Wood, C.; de Groot, M. J.; Leishman, D.; Sutcliffe, M. J.; Mitcheson, J. S. Drug binding interactions in the inner cavity of HERG channels: molecular insights from structure−activity relationships of clofilium and ibutilide analogs. *Mol. Pharmacol.* **2006**, *69*, 509–519.
(86) Siebrands, C. C.; Friederich, P. Structural requirements of human ether-a-go-go-related gene channels for block by bupivacaine. *Anesthesiology* **2007**, *106*, 523–531.
(87) Kamiya, K.; Niwa1, R.; Morishima1, M.; Honjo1, H.; Sanguinetti, M. C. Molecular determinants of hERG channel block by terfenadine and cisapride. *J. Pharmacol. Sci.* **2008**, *108*, 301–307.
(88) Afzelius, L.; Masimirembwa, C. M.; Karlén, A.; Andersson, T. B.; Zamora, I. Discriminant and quantitative PLS analysis of competitive CYP2C9 inhibitors versus noninhibitors using alignment independent GRIND descriptors. *J. Comput.-Aided Mol. Des.* **2002**, *16*, 443–458.
(89) Stansfeld, P. J.; Sutcliffe, M. J.; Mitcheson, J. S. Molecular mechanisms for drug interactions with hERG that cause long QT syndrome. *Expert Opin. Drug Metab. Toxicol.* **2006**, *2*, 81–94.
(90) Needham, M.; Sturgess, N.; Cerillo, G.; Green, I.; Warburton, H.; Wilson, R.; Martin, L.; Barratt, D.; Anderson, M.; Reilly, C.; Hollis, M. Monocyte chemoattractant protein-1: receptor interactions and calcium signaling mechanisms. *J. Leukoc. Biol.* **1996**, *60*, 793–803.
(91) Springthorpe, B.; Strandlund, G. Radiolabeled bispidine compound and assay for I_{Kr} potassium channel blocking activity. PCT Int. Appl. WO2005037052, **2005**, 22 pp.
(92) Murphy, S. M.; Palmer, M.; Poole, M. F.; Padegimas, L.; Hunady, K.; Danzig, J.; Gill, S.; Gill, R.; Ting, A.; Sherf, B.; Brunden, K.; Stricker-Krongrad, A. Evaluation of functional and binding assays in cells expressing either recombinant or endogenous hERG channel. *J. Pharm. Toxicol. Methods* **2006**, *54*, 42–55.
(93) Donovan, S. F.; Pescatore, M. C. Method for measuring the logarithm of the octanol−water partition coefficient by using short octadecyl-poly(vinyl alcohol) high-performance liquid chromatography columns. *J. Chromatogr. A* **2002**, *952*, 47–61.
(94) Box, K.; Elliott, S.; Cimpan, G. High throughput pKa and logD7.4 measurements. *PharmaChem* **2003**, *2*, 55–59.
(95) Zhou, Y.; MacKinnon, R. The occupancy of ions in the K^+ selectivity filter: Charge balance and coupling of ion binding to a protein conformational change underlie high conduction rates. *J. Mol. Biol.* **2003**, *333*, 965–975.